

No evidence for parity violation in BOSS

Alex Krolewski,^{a,b,c} Simon May,^{c,d} Kendrick Smith,^c
Hans Hopkins^{a,c}

^aDepartment of Physics and Astronomy, University of Waterloo
200 University Avenue West, Waterloo, ON N2L 3G1, Canada

^bWaterloo Centre for Astrophysics, University of Waterloo
200 University Avenue West, Waterloo, ON N2L 3G1, Canada

^cPerimeter Institute for Theoretical Physics
31 Caroline Street North, Waterloo, ON N2L 2Y5, Canada

^dDepartment of Physics, North Carolina State University
Raleigh, NC, 27695-8202, USA

E-mail: akrolews@uwaterloo.ca, simon.may@pitp.ca, kmsmith@pitp.ca,
hshopkins@uwaterloo.ca

Abstract. Recent studies have found evidence for parity violation in the BOSS spectroscopic galaxy survey, with statistical significance as high as 7σ . These analyses assess the significance of the parity-odd four-point correlation function (4PCF) with a statistic called χ^2 . This statistic is biased if the *parity-even* eight-point correlation function (8PCF) of the data differs from the mock catalogs. We construct new statistics χ^2_{\times} , χ^2_{null} that separate the parity violation signal from the 8PCF bias term, allowing them to be jointly constrained. Applying these statistics to BOSS, we find that the parity violation signal ranges from 0 to 2.5σ depending on analysis choices, whereas the 8PCF bias term is $\sim 6\sigma$. We conclude that there is no compelling evidence for parity violation in BOSS. Our new statistics can be used to search for parity violation in future surveys, such as DESI, without 8PCF biases.

Contents

1	Introduction	2
1.1	Background: Parity violation in BOSS?	2
1.2	The χ^2 statistic and the difficulty of modeling the 4PCF covariance	2
1.3	New statistics that distinguish parity violation and data–mock mismatch	5
2	BOSS data	7
2.1	Catalogs and weights	7
2.2	Sample definition: CMASS vs. CMASSLOWZTOT	8
3	Reproducing results from [1, 2]	9
3.1	The parity-odd four-point estimator $\widehat{\mathcal{E}}_a$	9
3.2	Computing the analytic covariance C_{ana}	11
3.3	Computing χ^2	13
4	The new statistics χ_{\times}^2 and χ_{null}^2	17
4.1	Splitting BOSS into patches	17
4.2	Definitions and notation	18
4.3	The statistic χ_{\times}^2	19
4.4	The statistic χ_{null}^2	20
4.5	Combined NGC + SGC significance	24
5	Discussion	25
A	Deriving the analytic covariance	30
A.1	Special function identities	30
A.2	Strategy of the calculation	31
A.3	Computing the two-point functions in eq. (A.15)	32
A.4	Computing $T_{l_1 l_2 l_3 l'_1 l'_2 l'_3}^{\beta_1 \beta_2 \beta_3 \beta'_1 \beta'_2 \beta'_3}$ and $U_{l_1 l_2 l_3 l'_1 l'_2 l'_3}^{\beta_1 \beta_2 \beta_3 \beta'_1 \beta'_2 \beta'_3}$	34
A.5	Numerical evaluation of the binned Bessel function $B_l^\beta(k)$	36
A.6	Convergence tests for the analytic covariance matrix	37
B	Why is $\text{Var}(\chi_{\times}^2)$ smaller than $\text{Var}(\chi^2)$?	38
B.1	A one-parameter model for $\text{Var}(\chi^2)$	38
B.2	A zero-parameter model for $\text{Var}(\chi_{\times}^2)$	39
B.3	Comparison between $\text{Var}(\chi^2)$ and $\text{Var}(\chi_{\times}^2)$	40
C	Data and mock investigations	40
D	Condition number and eigenvalues of the analytic covariance	41
E	Comments on related null tests from [1, 2]	42
E.1	Matching the 4PCF between data and mocks	43
E.2	Comparing χ^2 in different patches of sky	44
E.3	The r_p -statistic (correlating NGC and SGC)	44

1 Introduction

1.1 Background: Parity violation in BOSS?

Recently, two groups [1, 2] reported evidence for parity violation in the Baryon Oscillation Spectroscopic Survey (BOSS), following the proposal of [3] and using methods developed in [4]. In [1], statistical significance as high as 7.1σ was reported, and in [2] statistical significance as high as 2.9σ was reported.¹

Cosmological parity violation, if confirmed, would have profound implications for fundamental physics, and so the results of [1, 2] have attracted a great deal of interest.² A variety of models were proposed which generate parity violation on cosmological scales (e.g. [5–10] and references therein).

On the observational side, the situation has been puzzling. Follow-up searches in BOSS for specific parity-violating models of inflation produced null results [11]. A re-analysis of BOSS using a different set of mock catalogs shifted the detection significance of parity violation by around 2σ [12], suggesting that the analysis may not be very robust to the choice of mocks. In the cosmic microwave background (CMB), some analyses have found tentative evidence for parity violation (e.g. [13–15] and references therein) whereas others have found null results [16].

These follow-up studies may suggest that the original detection of parity violation is spurious. On the other hand, no follow-up study has directly refuted the 7σ detection from [1], so the current observational situation is unclear. (It is also unclear how to interpret results from future datasets, e.g. the Dark Energy Spectroscopic Instrument (DESI) survey [17], until the 7σ excess in BOSS is diagnosed.)

One may ask, is there a statistical procedure which will unambiguously determine whether the 7σ detection of parity violation in BOSS is spurious or not? In this paper, we develop such a procedure. We construct improved statistics (denoted χ_x^2 , χ_{null}^2) which separate the 7σ detection from [1] into two contributions: a parity violation contribution, and a “data–mock mismatch” contribution which is nonzero if the *parity-even* eight-point correlation function (8PCF) of the data differs from the mock catalogs.

We apply these statistics to BOSS data, and find that the parity violation signal is not statistically significant (significance varies between 0 to 2.5σ depending on analysis choices, see figures 5 and 6), whereas the data–mock mismatch signal is $\sim 6\sigma$. Our interpretation is that there is not compelling evidence for parity violation in BOSS.

Our new statistics χ_x^2 , χ_{null}^2 are conceptually simple, but the details are complicated, since algebraically messy objects arise, e.g. the parity-odd four-point correlation function (4PCF), eq. (3.3), and its analytic covariance (appendix A). In the rest of this extended introduction (sections 1.2 to 1.3), we present the main results of the paper in streamlined form. Details and derivations will be given in later sections (sections 2 to 5).

1.2 The χ^2 statistic and the difficulty of modeling the 4PCF covariance

The analysis in [1, 2] is based on a particular statistic applied to galaxy catalogs, denoted χ^2 and defined below, which is sensitive to parity violation. Statistical significance is assigned by

¹Refs. [1, 2] report different statistical significances mainly because a key analysis parameter N_β (number of radial bins in the χ^2 estimator) is chosen differently. In [1, 2], N_β is chosen to be 18, 10 respectively. (Note that [1] also presents results with $N_\beta = 10$, and these agree qualitatively with [2].) The parameter N_β is defined precisely in section 3.1.

²E.g. three recent workshops were devoted to parity violation: <https://events.asiaa.sinica.edu.tw/workshop/20231204/>, <https://inspirehep.net/seminars/2170834>, <https://parity.cosmodiscussion.com/>.

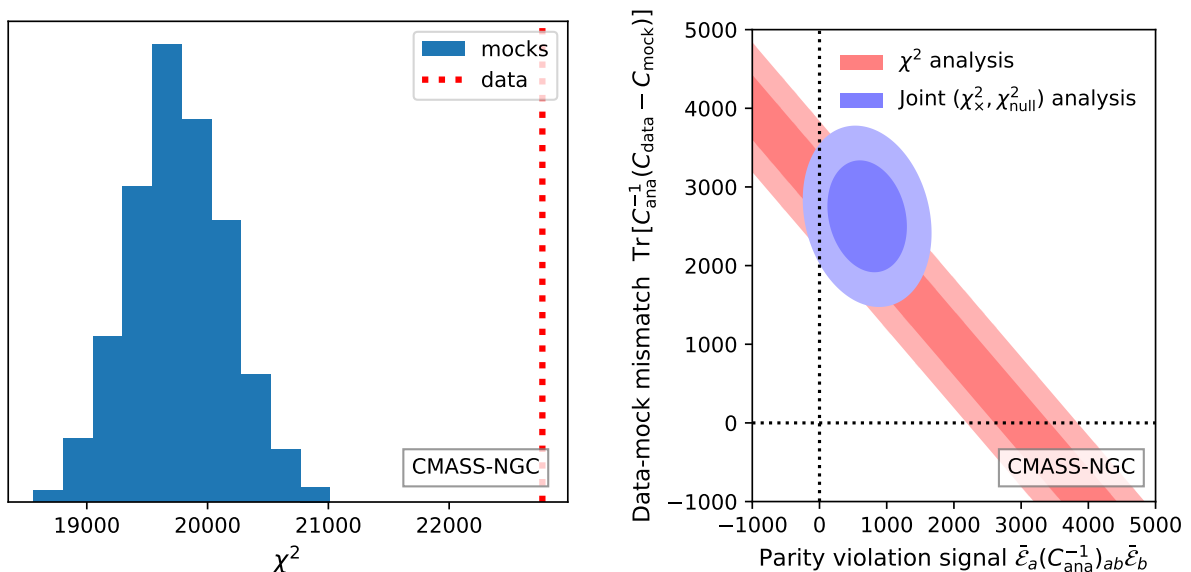


Figure 1. Analysis of parity violation in the BOSS CMASS-NGC dataset. (Results for CMASS-LOWZTOT-SGC are qualitatively similar and shown in section 4.) **Left panel.** When the χ^2 statistic defined in eq. (1.4) is evaluated on BOSS data (dashed vertical line), the result is a $\sim 7\sigma$ outlier relative to mock catalogs (solid histogram). This reproduces the main result from [1]. **Right panel.** We interpret this 7σ signal as a sum of parity violation and “data–mock mismatch” contributions (eq. (1.7)). If only χ^2 is used, these contributions are perfectly degenerate (red regions). The new statistics $\chi_x^2, \chi_{\text{null}}^2$ defined in eqs. (1.5) and (1.6) break this degeneracy (blue regions). We see that the parity violation signal drops to $< 2\sigma$, while the data–mismatch signal remains at high significance. Throughout this panel, statistical errors are assumed Gaussian, with covariance estimated from mock catalogs. Light/dark regions are 68% and 95% confidence levels (CL).

computing χ^2 on the BOSS data, and comparing it to χ^2 values from an ensemble of BOSS mock galaxy catalogs (as first proposed for the two-point correlation function in [18], applied to the three-point function in [19], and the parity-odd four-point function in [1]). Following [1, 2], we have used the MultiDark-PATCHY BOSS mock catalogs [20, 21] (or “PATCHY mocks” for short) throughout this paper. We have reproduced the result from [1] in the left panel of figure 1. We find that χ_{data}^2 is indeed a 7σ outlier, relative to a histogram of χ_{mock}^2 values. Here are three possible interpretations of this 7σ result:

1. *Parity-violating new physics:* The spatial clustering of galaxies in the universe is not parity-invariant.
2. *Parity-violating systematics:* BOSS has undiagnosed systematics which are not parity-invariant.
3. *Data–mock mismatch:* There is no evidence for parity violation (either physical or systematic) in BOSS, but the mocks do not perfectly model the *parity-even* higher N -point functions of the data. (More precisely, if the parity-even 8PCF of the mock catalogs differs from the data, then the mocks may underpredict the covariance of the 4PCF, leading to a biased χ^2 .)³

³This possibility is emphasized throughout [1, 2], where it is described as underestimating the covariance

To explore the “data–mock mismatch” possibility in more detail, we explain how χ^2 is defined. The steps are (schematically):

$$\left(\text{Galaxy catalog}\right) \rightarrow \left(\text{Parity-odd 4PCF } \widehat{\mathcal{E}}_a\right) \rightarrow \left(\text{Parity-even 8PCF } \chi^2\right) \quad (1.1)$$

The new quantities $\widehat{\mathcal{E}}_a$ and $(C_{\text{ana}})_{ab}$ will be defined precisely later (section 3). In the introduction, the following qualitative descriptions of $\widehat{\mathcal{E}}_a$ and $(C_{\text{ana}})_{ab}$ will suffice:

- Each component $a = 1, \dots, N_{\text{dof}}$ of $\widehat{\mathcal{E}}_a$ is a parity-odd four-point function in the galaxy catalog. “Parity-odd” means that if a spatial reflection is applied to the galaxy catalog, then $\widehat{\mathcal{E}}_a$ transforms as $\widehat{\mathcal{E}}_a \rightarrow -\widehat{\mathcal{E}}_a$. This implies:

$$\bar{\mathcal{E}}_a = 0 \quad \text{if the statistics of the galaxy field are parity-invariant} \quad (1.2)$$

where $\bar{\mathcal{E}}_a$ denotes the true (i. e. cosmic average) parity-odd four-point function $\widehat{\mathcal{E}}_a$.⁴

- The “analytic” covariance matrix $(C_{\text{ana}})_{ab}$ is the N_{dof} -by- N_{dof} matrix:

$$(C_{\text{ana}})_{ab} = \langle \widehat{\mathcal{E}}_a \widehat{\mathcal{E}}_b \rangle \quad \text{assuming that the galaxy field } \delta_g \text{ is Gaussian} \quad (1.3)$$

The assumption that δ_g is Gaussian is not intended to be an accurate approximation. It is only intended to give a calculable, well-motivated, invertible covariance matrix that can be used for data compression purposes when defining the χ^2 statistic:

$$\chi^2 \equiv \widehat{\mathcal{E}}_a (C_{\text{ana}}^{-1})^{ab} \widehat{\mathcal{E}}_b \quad (1.4)$$

Note that the definition (1.4) of χ^2 involves squaring the parity-odd 4PCF $\widehat{\mathcal{E}}_a$. Therefore, χ^2 is a parity-even eight-point statistic, whereas $\widehat{\mathcal{E}}_a$ is a parity-odd four-point statistic. This makes the χ^2 statistic more fragile: it can be biased by parity-even effects (whereas many observational systematics cannot generate a parity-odd signal). In particular, if the parity-even 8PCF of the mock catalogs does not agree with the data (“data–mock mismatch”), then there is no symmetry which protects the χ^2 statistic from bias. Quantitatively, a $\sim 20\%$ discrepancy between the parity-even 8PCF of the mocks and data would explain the results of [1, 2] without parity violation (either cosmological or systematic).

A priori, a $\sim 20\%$ 8PCF discrepancy between mocks and data is entirely plausible. The PATCHY mocks include free parameters (mostly pertaining to the galaxy–halo relation) which are adjusted so that the two-point correlation function (2PCF) of the mocks agrees with the data. The mocks are not intended to model higher-point correlation functions precisely.⁵

(or noise) of the statistic $\widehat{\mathcal{E}}_a$ (defined later in the paper). E. g. the abstract of [1] reads “Underestimation of the noise could also lead to a spurious detection”, and [2] writes “A spurious detection of parity-violation could be caused by the simulations underestimating the true covariance”. [1] estimated the impact of a wrong covariance matrix on the detection significance in their section 7.

⁴In most of the paper, we denote the parity-odd four-point function $\widehat{\mathcal{E}}_a$ using a single index $a = 1, \dots, N_{\text{dof}}$. However, the “natural” definition of $\widehat{\mathcal{E}}$ (section 3.1) is a six-index object $\widehat{\mathcal{E}}_{\ell_1 \ell_2 \ell_3}^{\beta_1 \beta_2 \beta_3}$, where β_i denotes a radial bin and $0 \leq \ell_i \leq 4$ denotes an “angular momentum” (index of the spherical harmonics). When we use the compressed notation $\widehat{\mathcal{E}}_a$, each value of the “flattened” index $a = 1, \dots, N_{\text{dof}}$ represents a different six-tuple $((\beta_i), (\ell_i))$. The number of components N_{dof} can be large. In figure 1, we have used an “18-bin” setup with $N_{\text{dof}} = 18768$. See section 3.1 for details.

⁵This is a natural consequence of the fact that large-scale structure (LSS) analyses have focused on the two-point function, and the massive catalogs of mocks necessary for this analysis have only been created for analyses of the large-scale power spectrum and correlation function. Large simulation suites devoted to higher-point statistics have only recently become available (e. g. Quijote [22]) and have not generally been used to create mocks for the BOSS survey, partially because the $1 h^{-1}$ Gpc boxes are smaller than the BOSS survey volume.

Indeed, the three-point correlation function (3PCF) of the PATCHY mocks generally agrees with the data [20, 23], but has some discrepancies [21]. In section 4.2.3 of [1] it is reported that the parity-even 4PCFs disagree at 4.9σ (for some choices of binning). Generally speaking, higher-point functions are sensitive to tails of distributions, and can magnify small modeling issues. Therefore, it seems completely plausible that the 8PCFs of the mocks and data could disagree by $\sim 20\%$.

(As an aside, squaring $\widehat{\mathcal{E}}_a$ seems to be necessary in an analysis where no model of the parity-odd 4PCF is assumed. On the other hand, if a model for $\widehat{\mathcal{E}}_a$ is assumed, then the optimal statistic is linear in $\widehat{\mathcal{E}}_a$, and 8PCF bias is not an issue. This may explain why model-based analyses have produced null results so far [11].)

1.3 New statistics that distinguish parity violation and data–mock mismatch

Now we can present the main idea of this paper. So far, we have proposed data–mock mismatch as a possible explanation for the 7σ signal in figure 1 (left panel), but we have not presented evidence for or against this possibility. We will now construct new statistics, denoted χ_x^2 and χ_{null}^2 , which cleanly separate parity violation from data–mock mismatch.

Our construction is based on the following simple idea. If χ^2 excess is due to parity violation, then the true parity-odd four-point function $\bar{\mathcal{E}}_a$ of the universe is nonzero. In this case, we should see the same (within statistical errors) parity-odd four-point function $\widehat{\mathcal{E}}_a$ in different parts of the sky. On the other hand, if the χ^2 excess is due to data–mock mismatch, then $\widehat{\mathcal{E}}_a$ has mean zero, but the mocks underestimate the covariance $\langle \widehat{\mathcal{E}}_a \widehat{\mathcal{E}}_b \rangle$. In this case, we should see uncorrelated (within statistical errors) parity-odd four-point functions $\widehat{\mathcal{E}}_a$ in different parts of the sky.

To make this idea precise, we start by splitting the BOSS survey area into N_p patches of roughly equal area, where $N_p = 3$ for the BOSS “Constant Stellar Mass” (CMASS) North Galactic Cap (NGC) dataset, denoted as CMASS-NGC (which we focus on in this introduction), and $N_p = 2$ for the CMASSLOWZTOT South Galactic Cap (SGC) dataset, denoted as CMASSLOWZTOT-SGC.⁶ We separate patches by gaps of 5–10 degrees, to make the patches approximately statistically independent. The patches are shown in section 4.1 and figure 3.

We estimate the parity-odd 4PCF independently in each patch $\mu = 1, \dots, N_p$, and denote the result by $\widehat{\mathcal{E}}_a^\mu$, now with an extra index μ . We then define new statistics:

$$\chi_x^2 \propto \sum_{\mu \neq \nu} \widehat{\mathcal{E}}_a^\mu (C_{\text{ana}}^{-1})^{ab} \widehat{\mathcal{E}}_b^\nu \quad (1.5)$$

$$\chi_{\text{null}}^2 \propto \sum_{\mu \neq \nu} (\widehat{\mathcal{E}}_a^\mu - \widehat{\mathcal{E}}_a^\nu) (C_{\text{ana}}^{-1})^{ab} (\widehat{\mathcal{E}}_b^\mu - \widehat{\mathcal{E}}_b^\nu) \quad (1.6)$$

(The overall normalizations of χ_x^2 and χ_{null}^2 will be defined in section 4.) At an intuitive level, we expect that χ_x^2 will only be sensitive to parity violation, and χ_{null}^2 will only be sensitive to data–mock mismatch, by the following argument:

- The χ_x^2 statistic measures correlations between parity-odd four-point functions $\widehat{\mathcal{E}}_a^\mu$ in different ($\mu \neq \nu$) patches of sky. Such correlations do not acquire expectation values from data–mock mismatch (which acts as “noise” that is uncorrelated between well-separated patches). On the other hand, if parity is violated, then $\bar{\mathcal{E}}_a$ is the same in all patches, leading to a nonzero expectation value $\langle \chi_x^2 \rangle \propto \bar{\mathcal{E}}_a (C_{\text{ana}}^{-1})^{ab} \bar{\mathcal{E}}_b$.

⁶We explain in section 2.2 why we consider two different samples in the northern and southern galactic caps.

- The χ_{null}^2 statistic defines a null test: it measures consistency between four-point functions in different parts of the sky. Parity violation does not contribute to χ_{null}^2 , since we still expect consistent values of $\hat{\mathcal{E}}_a$ in different parts of the sky. However, systematics or data–mock mismatch will add “noise” to $\hat{\mathcal{E}}_a$, which does contribute to χ_{null}^2 .

More formally, in section 4 we will show that the new statistics χ_{\times}^2 and χ_{null}^2 separate parity violation and data–mock mismatch, in the following precise sense. Going back to the original χ^2 statistic in eq. (1.4), we calculate the expectation value $\langle \chi^2 \rangle$ relative to mocks, and find two terms:

$$\langle \chi^2 \rangle_{\text{data}} - \langle \chi^2 \rangle_{\text{mock}} = \underbrace{\bar{\mathcal{E}}_a (C_{\text{ana}}^{-1})^{ab} \bar{\mathcal{E}}_b}_{\text{parity violation}} + \underbrace{\text{Tr}[(C_{\text{data}} - C_{\text{mock}})C_{\text{ana}}^{-1}]}_{\text{data–mock mismatch}} \quad (1.7)$$

The “parity violation” term in eq. (1.7) is nonzero if the true parity-odd four-point function $\bar{\mathcal{E}}_a$ of the universe is nonzero, and the “data–mock mismatch” term is nonzero if the covariance matrix $C_{ab} = \langle \hat{\mathcal{E}}_a \hat{\mathcal{E}}_b \rangle$ of the mocks differs from the data. We then show that:

$$\langle \chi_{\times}^2 \rangle_{\text{data}} - \underbrace{\langle \chi_{\times}^2 \rangle_{\text{mock}}}_{=0} = \underbrace{\bar{\mathcal{E}}_a (C_{\text{ana}}^{-1})^{ab} \bar{\mathcal{E}}_b}_{\text{parity violation}} \quad (1.8)$$

$$\langle \chi_{\text{null}}^2 \rangle_{\text{data}} - \langle \chi_{\text{null}}^2 \rangle_{\text{mock}} = \underbrace{\text{Tr}[(C_{\text{data}} - C_{\text{mock}})C_{\text{ana}}^{-1}]}_{\text{data–mock mismatch}} \quad (1.9)$$

Comparing with eq. (1.7), we see that the statistics χ_{\times}^2 and χ_{null}^2 formally separate parity violation from data–mock mismatch, as argued intuitively above.

The idea of χ_{\times}^2 was inspired by a standard trick from CMB data analysis. The most straightforward way to estimate a CMB power spectrum C_l would be to make a single CMB map, take its auto power spectrum, and subtract the noise bias N_l . In practice, this is not robust since the noise bias N_l is difficult to model. A more robust approach is to cross-correlate maps with independent noise realizations (e.g. made from data taken at different times), so that there is no noise bias N_l to subtract. Analogously, in this paper we obtain independent estimates of the parity-odd 4PCF, by computing $\hat{\mathcal{E}}_a$ in different parts of the sky. By cross-correlating these measurements, we obtain a statistic χ_{\times}^2 with no bias $\langle \chi_{\times}^2 \rangle_{\text{mock}}$ to subtract.

In the right panel of figure 1, we apply the statistics χ_{\times}^2 and χ_{null}^2 to BOSS. The parity violation signal drops to $< 2\sigma$, while the data-mismatch signal remains at high significance. Our interpretation is that there is not compelling evidence for parity violation in BOSS (for the CMASS-NGC sample – see figures 5 and 6 for SGC and NGC+SGC results).

In this introduction, we explained the main ideas of our analysis, glossing over technical details. In the rest of the paper, we will fill in the details. In section 2, we describe the BOSS data and mock catalogs, and details of our processing. In section 3 we define the χ^2 statistic, and reproduce the $\sim 7\sigma$ and $\sim 3\sigma$ results from [1, 2]. In section 4, we define the new statistics χ_{\times}^2 and χ_{null}^2 , derive their main properties, and apply them to BOSS. We conclude in section 5. We make our data products publicly available.⁷

⁷Our data can be accessed here: <https://doi.org/10.5281/zenodo.12537418>.

2 BOSS data

2.1 Catalogs and weights

We measure the parity-odd four-point function using the publicly available BOSS DR12 galaxy catalogs [24–26].⁸ We use the same fiducial cosmology as BOSS to convert angles and redshifts into Cartesian coordinates [27]: $\Omega_m = 0.31$, $\Omega_b h^2 = 0.022$, $h = 0.676$, $\sigma_8 = 0.8$, $n_s = 0.96$, and $\Sigma m_\nu = 0.06$ eV. We compare the parity-odd signal in data to the parity-odd signal in 2048 MultiDark-Patchy mocks [20, 21],⁹ run with the parameter set $\Omega_m = 0.3071$, $\Omega_b h^2 = 0.02205$, $h = 0.6777$, $\sigma_8 = 0.8288$, $n_s = 0.96$, and $\Sigma m_\nu = 0$ eV. The mocks were produced using an approximate (fast) simulation based on second-order Lagrangian perturbation theory (2LPT) on large scales, and spherical collapse on small scales [28]. The parameters were tuned to match an abundance-matched N -body simulation, which itself matches the two-point BOSS clustering [21]. The mocks were then cut to the BOSS survey geometry, and coordinates were converted to Cartesian using the BOSS fiducial cosmology. (We also noticed a previously unknown systematic in the PATCHY mocks, described in appendix C, but we do not believe that it significantly affects the χ^2 statistic.)

In the data catalogs, galaxies are assigned weights $w_{g,\text{data}}$ to correct for imaging systematics w_{sys} (the product of weights correcting for dependence on stellar density and seeing); fiber collisions w_{cp} ; and redshift failures w_{noz} [29]; as well as Feldman–Kaiser–Peacock (FKP) weights $w_{\text{FKP}} = 1/(1 + n(z)P_0)$ [30] using the observed comoving number density $n(z)$ and $P_0 = 10^4 h^{-3} \text{Mpc}^3$.

$$w_{g,\text{data}} = (w_{\text{noz}} + w_{\text{cp}} - 1)w_{\text{sys}}w_{\text{FKP}} \quad (2.1)$$

w_{noz} and w_{cp} are both nearest-neighbor weights that transfer weights from redshift failures or fiber-collided galaxies to the nearest observed neighbor, with default values of 1; thus the proper way to combine them is $(w_{\text{noz}} + w_{\text{cp}} - 1)$ to ensure that observed galaxies are given weight 1. Random catalogs are generated uniformly within the BOSS imaging region, without fluctuations due to imaging systematics or redshift-dependent effects; hence randoms are only weighted by the FKP weights.

$$w_{r,\text{data}} = w_{\text{FKP}} \quad (2.2)$$

The mock weighting scheme is slightly different; mock galaxies are assigned weights

$$w_{g,\text{mock}} = w_{\text{cp}}w_{\text{veto}}w_{\text{FKP}} \quad (2.3)$$

Fiber collisions are implemented in mocks following the approximate method of [31] (randomly sub-sampling potentially collided galaxies, based on the number of tiles of coverage at a given point on the sky), rather than running the fiber assignment algorithm on the mocks. Close-pair weights w_{cp} are applied in the same way to mocks as to data. Since the mocks do not have redshift failures, there is no need for the $w_{\text{noz}} - 1$ term. Also, the mocks come with a binary veto flag w_{veto} to remove objects within the veto mask, whereas the veto mask (i. e. bright stars, poor imaging, etc.) has already been applied to the publicly available data products. Finally, the random weighting is slightly different in the mocks compared to the data: unlike

⁸<https://data.sdss.org/sas/dr12/boss/lss/>

⁹Described at <https://www.skiesanduniverses.org/page/page-3/page-15/page-9/>. We use the mocks available at https://data.sdss.org/sas/dr12/boss/lss/dr12_multidark_patchy_mock/ for CMASS-LOWZTOT, and the “pre-reconstruction” – i. e. without baryon acoustic oscillations (BAO) reconstruction applied – mocks (`Patchy_precon.tar.gz`) available at <https://www.ub.edu/bispectrum/page11.html> for CMASS.

the data randoms, the mock randoms are run through fiber assignment, and thus must also have close-pair weights applied

$$w_{r,\text{mock}} = w_{\text{cp}} w_{\text{FKP}} \quad (2.4)$$

There are various choices of random catalogs of differing density. We use randoms with $50\times$ the galaxy density: the “`random0`” catalog on data, the $50\times$ random catalog for Patchy CMASSLOWZTOT, and randomly subsampling the $100\times$ random catalog for Patchy CMASS. Choosing different random catalogs (i. e. using $50\times$ randoms for Patchy CMASS, or $100\times$ randoms on mocks and combining “`random0`” and “`random1`” on data) changes our results by $\sim 0.5\sigma$.

2.2 Sample definition: CMASS vs. CMASSLOWZTOT

BOSS galaxies are typically split in two ways [29]: by targeting algorithm, LOWZ or CMASS, or by redshift bin (after combining LOWZ and CMASS into the “CMASSLOWZTOT” sample), dubbed `z1`, `z2`, and `z3` in [32], at $0.2 < z < 0.5$, $0.4 < z < 0.6$, and $0.5 < z < 0.75$, respectively. LOWZ and CMASS were targeted as distinct samples. This leads to differences in their geometric coverage. In particular, a targeting error in early LOWZ data led to lower density in three regions in the North Galactic Cap (see appendix A and figure 8 in [29]; figure 8 shows the LOWZ region excluding these areas with lower density). These early data are referred to as “LOWZE2” and “LOWZE3” (after the two different targeting algorithms used), and are included in the combined “CMASSLOWZTOT” sample, since the error is known and can be propagated into a reduced number of randoms and different FKP weights. Finally, the imaging systematic weights are different for LOWZ and CMASS: no angular weights are applied to LOWZ, since the targets are brighter and do not show significant variation with seeing or stellar density.¹⁰

The different possible choices for the samples introduce additional options into our analysis. However, due to the associated computational cost, it is not straightforward to simply run all possibilities. In the following, we will describe the rationale behind our choices.

For the analysis with 10 radial bins ($N_\beta = 10$, see section 3.1), we match [2] and use CMASSLOWZTOT for both NGC and SGC, restricted to $0.43 < z < 0.7$.¹¹ For the case of 18 radial bins ($N_\beta = 18$, see section 3.1), we test the impact of varying the sample definition on the parity-odd detection, to test if it is affected by the targeting inhomogeneities in LOWZ, or by the different treatment of systematic weights in CMASS versus LOWZ.

Since the targeting inhomogeneities are only present in the NGC, our default 18-bin analysis uses CMASS only in the NGC, and CMASSLOWZTOT in the SGC, where we can benefit from the higher number density without potentially adding systematics due to the LOWZ inhomogeneity. Both are cut to the same redshift range $0.43 < z < 0.70$, matching the redshift cut in [1, 2]. The sample selection in the NGC thus matches that of [1], who use CMASS in both hemispheres (J. Hou and Z. Slepian, priv. comm). This is a conservative choice, in the sense that BOSS has released large-scale structure catalogs (and mocks) for CMASSLOWZTOT with randoms that correctly follow LOWZ’s angular variation; however, the impacts of these choices have only been validated on the large-scale two-point functions [32], and the possibility remains that higher-point functions are more sensitive to these choices.

¹⁰However, LOWZE3 does require angular weights depending on the seeing, due to the incorrect application of the CMASS star-galaxy separation [32].

¹¹The sample selection was described in more detail in the preceding paper on the parity-even four-point function [33].

Nevertheless, we find consistent detections of the 18-bin parity-odd four-point functions between both CMASS and CMASSLOWZTOT and between NGC and SGC, suggesting that these issues in sample construction are not responsible for the detection.

Summarizing, for the 18-bin case (analogous to [1]) we will consider two galaxy samples CMASS-NGC and CMASSLOWZTOT-SGC, restricted to $0.43 < z < 0.7$, and with per-object weights given by eqs. (2.1) to (2.4). For the 10-bin case (analogous to [2]), we will use CMASSLOWZTOT-NGC and CMASSLOWZTOT-SGC, again restricted to $0.43 < z < 0.7$, and with per-object weights given by eqs. (2.1) to (2.4).

3 Reproducing results from [1, 2]

In this section we will define the χ^2 statistic, and reproduce the $\sim 7\sigma$ and $\sim 3\sigma$ results from [1, 2]. This section mostly reviews results from previous papers, especially [1, 2, 4, 34], but is included to establish consistency between our pipeline and previous results, and to make our paper self-contained.

3.1 The parity-odd four-point estimator $\hat{\mathcal{E}}_a$

As described in the introduction, the first step in our pipeline is a parity-odd four-point estimator $\hat{\mathcal{E}}$, which we will sometimes denote as a six-index object $\hat{\mathcal{E}}_{l_1 l_2 l_3}^{\beta_1 \beta_2 \beta_3}$, and sometimes denote with a single “flattened” index $\hat{\mathcal{E}}_a$. Each value of the flattened index $a = 1, \dots, N_{\text{dof}}$ corresponds to one six-tuple $((\beta_i), (l_i))$. In this section, we will review the definition and key properties of $\hat{\mathcal{E}}$ from [1, 2, 4, 34].

For simplicity, our discussion of $\hat{\mathcal{E}}$ in this section assumes a simplified box geometry with periodic boundary conditions, no window function, and no lightcone evolution. To generalize to a realistic survey geometry, we use the edge correction procedure described in section 2 of [1] or section II.C of [2]. This edge correction is implemented in the ENCORE software [35], which we use to compute $\hat{\mathcal{E}}$ in our pipeline.

The input to $\hat{\mathcal{E}}$ is a galaxy field $\delta_g(\mathbf{x})$ defined by the usual “data minus randoms” prescription [35–37]:

$$\delta_g(\mathbf{x}) = \left(\frac{1}{n_{\text{gal}}} \sum_{i \in \text{gal}} \delta^3(\mathbf{x} - \mathbf{x}_i) \right) - \left(\frac{1}{n_{\text{rand}}} \sum_{j \in \text{rand}} \delta^3(\mathbf{x} - \mathbf{x}_j) \right) \quad (3.1)$$

To write down the definition of $\hat{\mathcal{E}}$, we will use six-index notation $\hat{\mathcal{E}}_{l_1 l_2 l_3}^{\beta_1 \beta_2 \beta_3}$. Here, each index $l_i \geq 0$ is an integer, and each index β_i is a non-overlapping radial bin of the form $[R_{\text{min}}, R_{\text{max}}]$. We define the function $W_{lm}^\beta(\mathbf{r})$, where the interval $\beta = [R_{\text{min}}, R_{\text{max}}]$ is a radial bin, by:

$$W_{lm}^\beta(\mathbf{r}) = \begin{cases} 4\pi Y_{lm}^*(\hat{\mathbf{r}})/V_\beta & \text{if } |r| \in \beta \\ 0 & \text{otherwise} \end{cases} \quad \text{where } V_\beta = \frac{4\pi}{3} (R_{\text{max}}^3 - R_{\text{min}}^3) \quad (3.2)$$

and Y_{lm} are the spherical harmonics. We define the estimator $\hat{\mathcal{E}}_{l_1 l_2 l_3}^{\beta_1 \beta_2 \beta_3}$ by:

$$\hat{\mathcal{E}}_{l_1 l_2 l_3}^{\beta_1 \beta_2 \beta_3} = \frac{(-1)^{\sum l_i}}{V_{\text{fid}}} \sum_{m_1 m_2 m_3} \begin{pmatrix} l_1 & l_2 & l_3 \\ m_1 & m_2 & m_3 \end{pmatrix} \int d^3 \mathbf{x} \delta_g(\mathbf{x}) \left(\prod_{i=1}^3 \int d^3 \mathbf{r}_i W_{l_i m_i}^{\beta_i}(\mathbf{r}_i) \delta_g(\mathbf{x} + \mathbf{r}_i) \right) \quad (3.3)$$

where V_{fid} is a fiducial survey volume (see table 1). The estimator $\hat{\mathcal{E}}_{l_1 l_2 l_3}^{\beta_1 \beta_2 \beta_3}$ defined by eq. (3.3) has the following properties:

- $\widehat{\mathcal{E}}_{l_1 l_2 l_3}^{\beta_1 \beta_2 \beta_3}$ is a four-point estimator in the galaxy field $\delta_g(\mathbf{x})$.
- $\widehat{\mathcal{E}}_{l_1 l_2 l_3}^{\beta_1 \beta_2 \beta_3}$ is invariant under rotations of the coordinate system.
- $\widehat{\mathcal{E}}_{l_1 l_2 l_3}^{\beta_1 \beta_2 \beta_3}$ is nonzero if and only if the triangle inequality $|l_1 - l_2| \leq l_3 \leq (l_1 + l_2)$ is satisfied.
- $\widehat{\mathcal{E}}_{l_1 l_2 l_3}^{\beta_1 \beta_2 \beta_3}$ is either parity-even or parity-odd, depending on whether $(l_1 + l_2 + l_3)$ is even or odd.
- $\widehat{\mathcal{E}}_{l_1 l_2 l_3}^{\beta_1 \beta_2 \beta_3}$ is either real or imaginary, depending on whether $(l_1 + l_2 + l_3)$ is even or odd.
- $\widehat{\mathcal{E}}_{l_1 l_2 l_3}^{\beta_1 \beta_2 \beta_3}$ is either symmetric or antisymmetric under permutations of (β_i, l_i) , depending on whether $(l_1 + l_2 + l_3)$ is even or odd:

$$\widehat{\mathcal{E}}_{l_1 l_2 l_3}^{\beta_1 \beta_2 \beta_3} = (-1)^{\sum l_i} \widehat{\mathcal{E}}_{l_2 l_1 l_3}^{\beta_2 \beta_1 \beta_3} = (-1)^{\sum l_i} \widehat{\mathcal{E}}_{l_1 l_3 l_2}^{\beta_1 \beta_3 \beta_2} \quad (3.4)$$

Since we are interested in the parity-odd case, we will only consider components of $\widehat{\mathcal{E}}$ such that $\sum l_i$ is odd. In view of the permutation symmetry (3.4), we will also assume $\beta_1 \leq \beta_2 \leq \beta_3$.

Additionally, in [1] all three radial bins must be distinct ($\beta_1 < \beta_2 < \beta_3$), and in [2] they must be separated by at least one bin ($\beta_1 + 2 < \beta_2 + 1 < \beta_3$), in order to reduce dependence on nonlinear scales. We will cover both cases by introducing a parameter Δ , and requiring

$$(\beta_1 + 2\Delta) < (\beta_2 + \Delta) < \beta_3 \quad (3.5)$$

where $\Delta = 0, 1$ in refs. [1, 2] respectively.

Summarizing, the parity-odd four-point function $\widehat{\mathcal{E}}_{l_1 l_2 l_3}^{\beta_1 \beta_2 \beta_3}$ has one component for each six-tuple $((\beta_i), (l_i))$ such that $\sum l_i$ is odd, the triangle inequality $|l_1 - l_2| \leq l_3 \leq (l_1 + l_2)$ is satisfied, and the bin constraint (3.5) is satisfied. A short calculation gives the following general formula for the number of components N_{dof} , as a function of $(N_\beta, l_{\text{max}}, \Delta)$:

$$N_{\text{dof}} = \underbrace{\left(\frac{(N_\beta - 2\Delta)(N_\beta - 2\Delta - 1)(N_\beta - 2\Delta - 2)}{6} \right)}_{\substack{\text{number of triples } (\beta_1, \beta_2, \beta_3) \\ \text{such that } (\beta_1 + 2\Delta) < (\beta_2 + \Delta) < \beta_3}} \times \underbrace{\left\lfloor \frac{2l_{\text{max}}^3 + 3l_{\text{max}}^2 + 2l_{\text{max}} + 4}{8} \right\rfloor}_{\substack{\text{number of triples } (l_1, l_2, l_3) \\ \text{such that } l_1 + l_2 + l_3 \text{ is odd, and} \\ \text{triangle inequality is satisfied}}} \quad (3.6)$$

where the notation $\lfloor x \rfloor$ means “ x rounded down to an integer”. In this paper, we will focus on the following specific cases:

- A “10-bin” case following [2]: We use $N_\beta = 10$ linearly spaced radial bins in the interval $[20, 160] h^{-1}$ Mpc, with $(l_{\text{max}}, \Delta) = (4, 1)$. Then eq. (3.6) gives $N_{\text{dof}} = 1288$. (Note that our “10-bin” case is the same as the 10-bin analysis from [2] which uses $\Delta = 1$, but not the same as the 10-bin analysis from [1] which uses $\Delta = 0$.)
- An “18-bin” case following [1]: We use $N_\beta = 18$ linearly spaced radial bins in the interval $[20, 160] h^{-1}$ Mpc, with $(l_{\text{max}}, \Delta) = (4, 0)$. Then eq. (3.6) gives $N_{\text{dof}} = 18768$. (This differs slightly from the setup in [1], which uses bins in $[20, 164] h^{-1}$ Mpc.)

Reference	Bins	Dataset	$P_0 / h^{-3} \text{Mpc}^3$	$V_{\text{fid}} / h^{-3} \text{Gpc}^3$
[1]	18	CMASS-NGC	$1/(1.40 \times 10^{-4})$	2.50
		CMASSLOWZTOT-SGC	$1/(1.40 \times 10^{-4})$	0.790
[2]	10	CMASSLOWZTOT-NGC	$1/(3.19 \times 10^{-4})$	1.90
		CMASSLOWZTOT-SGC	$1/(3.16 \times 10^{-4})$	0.766

Table 1. Input parameters for the analytic covariance (section 3.2) in different cases, following [1, 2]. We note that the values of P_0 and V_{fid} are taken directly from [1, 2], where they are determined from fits of the analytic covariance matrix to that of the mocks. They do *not* therefore represent the actual number density or volume of the CMASS and CMASSLOWZTOT samples.

To compute $\hat{\mathcal{E}}$, we run the public ENCORE software [35] adapting the shell script available in the GitHub repository.¹² The strategy is to reduce the runtime by splitting the randoms into 32 equal files (after first randomizing their order to ensure that each random subset covers the full area). Then we compute counts of data powers D^N (with $N = 4$ for the four-point function), random powers R^N for the first random subset (for later use in edge correction), and data minus random powers $(D - R)^N$ for all 32 subsets. Note that the random catalogs are identical for each of the 2048 Patchy mocks, and hence we only generate them for the first Patchy mock. The random weights are automatically balanced to ensure that $\sum(D - R) = 0$ in the $(D - R)^N$ step; however, this re-weighting must also be applied to the first random subset used to calculate R^N counts. Hence, we re-create the first random subset for each Patchy mock, but with the weights rescaled to ensure that they match the sum of the corresponding Patchy mock’s data weights.

After the counts are combined into the two-point, three-point, and (parity-odd) four-point functions, edge correction is performed. Before and during edge correction, we keep both parity-even and parity-odd 4PCFs with $l_{\text{max}} = 5$. After edge correction, we keep only parity-odd 4PCFs with $l_{\text{max}} = 4$.

3.2 Computing the analytic covariance C_{ana}

Consider the covariance matrix $\text{Cov}(\hat{\mathcal{E}}_a, \hat{\mathcal{E}}_b)$, where $\hat{\mathcal{E}}_a$ is the parity-odd four-point estimator defined in the previous section. In [1], it was shown that this covariance matrix can be computed analytically under two simplifying approximations: the galaxy field $\delta_g(\mathbf{x})$ is a Gaussian field, and the survey geometry is a 3D periodic box with volume V_{fid} (i. e. neglecting lightcone evolution and anisotropic power spectra from redshift space distortions).

Throughout this paper, we define the “analytic” covariance matrix $(C_{\text{ana}})_{ab}$ to be the covariance computed under these approximations. Note that these approximations are not particularly good, and C_{ana} is not necessarily a good approximation to the true covariance C_{data} . This is not a problem, since in this paper we only use C_{ana} for data compression purposes, when defining statistics such as $\chi^2 = \hat{\mathcal{E}}_a (C_{\text{ana}}^{-1})^{ab} \hat{\mathcal{E}}_b$.

In appendix A, we give a self-contained derivation of the analytic covariance (re-deriving results from [4]). The input parameters and main computational steps can be summarized as follows:

- Following [1, 2], the galaxy power spectrum $P_g(k)$ is modelled using CLASS-PT [38] at redshift $z = 0.57$, and a Poisson noise term P_0 is added by hand.¹³ The specific values

¹²https://github.com/oliverphilcox/encore/blob/master/run_npcf.csh

¹³The power spectrum $P_{g,\text{CLASS-PT}}(k)$ was provided to us by Oliver Philcox, and was also used in [2]. The

of P_0 used vary with each considered case, and match those given in [1, 2] (where they were obtained by fitting the analytic covariance to the mock covariance). These values are summarized in table 1 and do not necessarily match the number density of each sample.

- Following [4], we apply a Gaussian damping to the power spectrum:

$$P_g(k) = (P_{g,\text{CLASS-PT}}(k) + P_0) \exp(-(k/k_0)^2) \quad \text{where } k_0 = 1 \text{ h Mpc}^{-1}. \quad (3.7)$$

- The fiducial effective survey volume appears in C_{ana} via an overall prefactor $1/V_{\text{fid}}$. As with P_0 , the values of this volume are different in each considered case, matching those from the fits in [1, 2], and are summarized in table 1, again, not necessarily matching the actual survey volume.
- The first computational step is computing a large number of correlation functions, for example the standard galaxy correlation function

$$\xi(r) = \int_0^\infty dk \frac{k^2}{2\pi^2} P_g(k) j_0(kr) \quad (3.8)$$

and additionally some non-standard correlation functions $H_l^\beta(r)$, $F_{l'l}^{\beta\beta'}(r)$ defined using similar k -integrals (see eqs. (A.22) and (A.24)). Following section 5.1 of [4], we do these k -integrals by summing over $N_k = 5000$ linearly spaced k -values with $k_{\text{min}} = 10^{-4} \text{ h Mpc}^{-1}$, $k_{\text{max}} = 5 \text{ h Mpc}^{-1}$.¹⁴

- The matrix elements of C_{ana} are given by integrals involving correlation functions computed in the previous step. For example, eq. (A.28) contains an integral of the form:

$$\int_0^\infty dr r^2 \xi(r) F_{l_1 l_1'}^{\beta_1 \beta_1'}(r) F_{l_2 l_2'}^{\beta_2 \beta_2'}(r) F_{l_3 l_3'}^{\beta_3 \beta_3'}(r) \quad (3.9)$$

Following section 5.1 of [4], we do these r -integrals by summing over $N_r = 4100$ linearly spaced r -values with $r_{\text{min}} = 10^{-5} \text{ Mpc h}^{-1}$, $r_{\text{max}} = 1000 \text{ Mpc h}^{-1}$.

We wrote a publicly available Julia software package to compute C_{ana} given the above inputs.¹⁵ Although some of the code used in [4] is also publicly available,¹⁶ we opted to create an independent implementation for several reasons:

- The public version of the code from [4] is only applicable to the calculation of the parity-even part of the analytic covariance (see appendix A for details), so it could not directly be used in the parity-odd analysis.
- In order to rule out any issues with the analysis related to the computation of C_{ana} , an independent implementation is very valuable, especially considering the complexity of the calculation and the mathematical objects involved.

CLASS-PT bias parameters were obtained by fitting the measured CMASS galaxy power spectra. This power spectrum file is included in our public code repository at <https://gitlab.com/Socob/analytic4pc>.

¹⁴These settings were derived from convergence tests performed on the analytic three-point function covariance in Section 6.5 of [19].

¹⁵Our code is available at <https://gitlab.com/Socob/analytic4pc>.

¹⁶https://github.com/Moctobers/npcf_cov

- Since the calculation is quite computationally intensive for larger numbers of bins, there was a large motivation to make full use of parallel computing resources in order to improve run time.
- In order to perform various tests of numerical stability and convergence, we wanted to create a flexible code that allows easily varying the numerical parameters (e. g. N_k , k_{\max}) without modifying the code itself.

In principle, the calculation of C_{ana} is an “embarrassingly parallel” problem, since each matrix element can be computed independently. However, an important part of the calculation involves caching the values of intermediate quantities, namely the ordinary and binned Bessel functions, $j_l(x)$ and $B_l^\beta(k)$, as well as the correlation functions $\xi(r)$, $H_l^\beta(r)$, $F_{ll'}^{\beta\beta'}(r)$, and combinatorial factors. Since these same quantities appear many times even for different covariance matrix elements, it would be immensely inefficient to re-compute them every time. This complicates parallelization, as naïvely running a serial code in parallel for different matrix elements would not only duplicate the cost of computing the cache for each instance, but also run into memory limitations since the size of these objects is not insignificant.

Our code makes use of Julia’s built-in distributed computing module `Distributed.jl`, which allows it to run in parallel on an arbitrary number of computing cores across several machines without being limited to a single shared-memory node, and without requiring the installation of additional libraries or software. The cache of intermediate quantities is implemented within each shared-memory machine via shared process memory in order to avoid storing multiple copies of the same data.

We have performed cross-checks of our code’s output with the public code from [4] and the related 10-bin covariance matrix used in [2], and have found excellent agreement approaching numerical precision. Further details of investigations concerning the numerical accuracy of the analytic covariance computation are laid out in appendix A. For instance, the integration parameters $(N_k, k_{\max}, N_r, r_{\max})$ should be chosen conservatively enough that the integrals converge. In appendix A.6, we present an “end-to-end” check which shows that all matrix entries of C_{ana} have converged, if we use the parameter choices above. In appendix D, we show that C_{ana} can be poorly conditioned, but this does not seem to be an issue for the χ^2 analysis.

3.3 Computing χ^2

Following [1, 2], we define the χ^2 statistic by:

$$\chi^2 \equiv \widehat{\mathcal{E}}_a (C_{\text{ana}}^{-1})^{ab} \widehat{\mathcal{E}}_b \quad (3.10)$$

The purpose of the χ^2 statistic is to provide data compression: it reduces the many-component parity-odd 4PCF $\widehat{\mathcal{E}}_a$ to a scalar quantity χ^2 .¹⁷

Our goal in this section is to reproduce the main results of [1, 2], by evaluating χ^2 on BOSS data and mocks, before defining new statistics χ_{\times}^2 , χ_{null}^2 in later sections. Our main results are shown in figure 2 and the rest of this section will be devoted to interpretation and discussion.

¹⁷Refs. [1, 2] also explore other forms of data compression, such as limiting the number of eigenvalues N_{eig} in the covariance, or using the mock covariance instead of the analytic covariance. In this paper, we choose to only use the χ^2 statistic defined in eq. (3.10), since it leads to the highest detection significance in [1, 2].

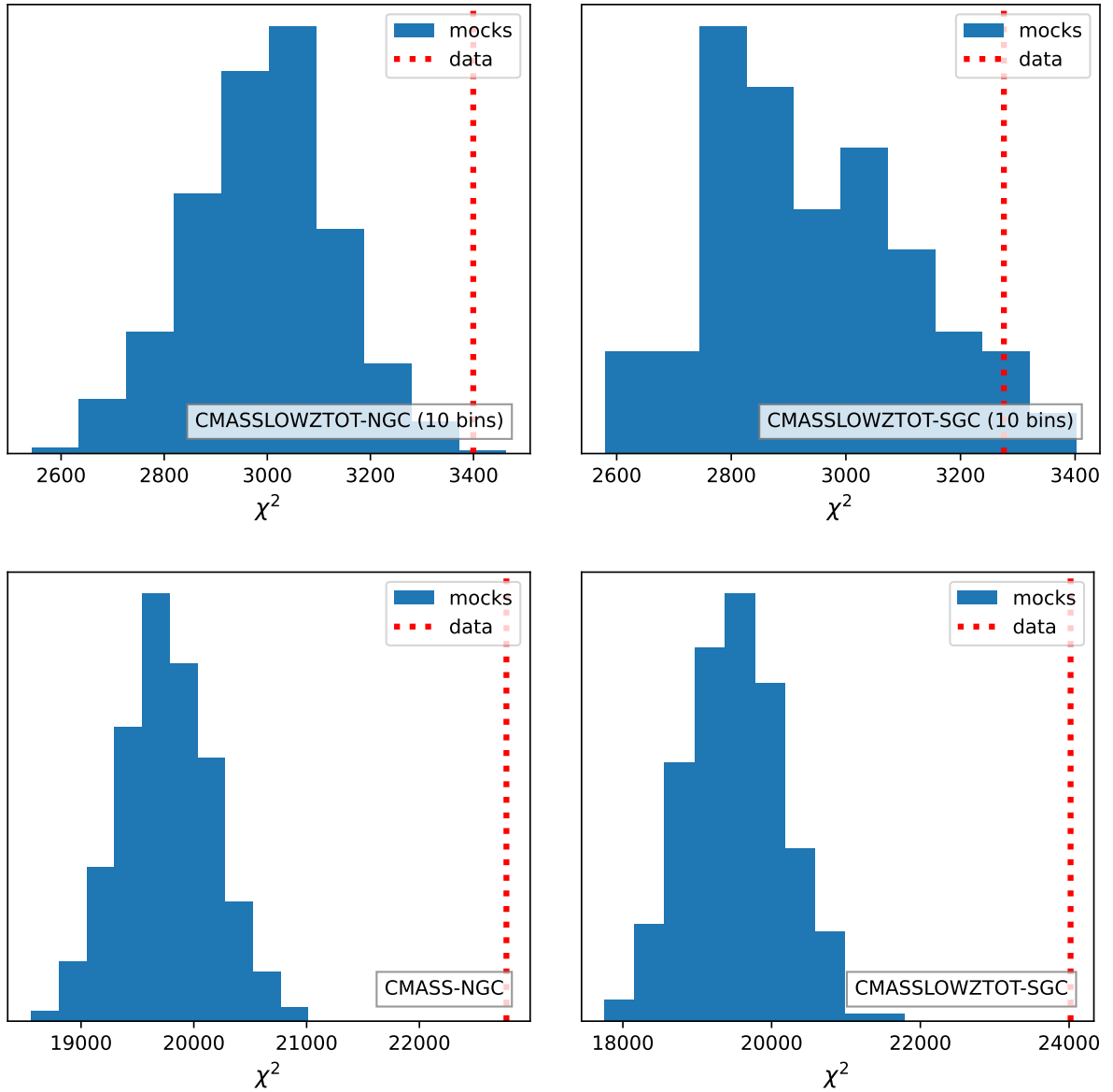


Figure 2. Reproducing results from [1, 2], by evaluating χ^2 on BOSS data (vertical dashed lines) and mocks (solid histograms). **Top row.** A 10-bin analysis following [2]. We find 2.8σ for CMASSLOWZTOT-NGC (top left) and 1.9σ for CMASSLOWZTOT-SGC (top right). **Bottom row.** An 18-bin analysis following [1]. We find 7.3σ for CMASS-NGC (bottom left) and 6.9σ for CMASSLOWZTOT-SGC (bottom right).

Analysis choice	10-bin, NGC	18-bin, NGC	18-bin, SGC
This work, baseline	2.8	7.3	6.9
Previous work: [1, 2]	2.4	4.7	5.4
Swap CMASS and CMASSLOWZTOT	–	5.4	9.2
Double \bar{n} in analytic covariance	–	–	8.1
Halve \bar{n} in analytic covariance	–	–	5.5
Turn off w_{noz}	–	4.3	–
Turn off w_{cp}	–	8.9	–
Turn off w_{sys}	3.0	–	–

Table 2. Detection significance of the parity-odd four point function using χ^2 , in number of Gaussian σ . Top rows compare our baseline results to those of [1, 2], and subsequent rows consider swapping the galaxy samples used in the 18-bin case between CMASS and CMASSLOWZTOT; changing the number density in the analytic covariance; and turning off various systematic weights. We perform these tests on one hemisphere and choice of N_β to illustrate their effect, which is expected to be similar for all three choices of N_β and hemisphere.

We note that the overall normalization of χ^2 is arbitrary, since χ^2 is proportional to the fiducial survey volume V_{fid} , and we chose V_{fid} (table 1) without a precise χ^2 normalization in mind. On a related note, χ^2 is not precisely χ^2 -distributed, for two reasons: $\hat{\mathcal{E}}_a$ is not a multivariate Gaussian, and C_{ana} does not perfectly model C_{mock} . (Similar comments apply to the new statistics χ^2_{\times} , χ^2_{null} in the next section.)

Therefore, throughout the paper, we assess statistical significance by comparing to a histogram of mocks. This procedure does not assume an analytic distribution for χ^2 , and is independent of the overall normalization of χ^2 . When we report statistical significance as a “number of sigmas” $S\sigma$, we report $S = (\chi^2_{\text{data}} - \langle \chi^2 \rangle_{\text{mock}}) / \text{Var}(\chi^2)_{\text{mock}}^{1/2}$, rather than reporting the p -value of the data within the mock distribution. This makes the approximation that the mock distribution is Gaussian, but lets us quantify large outliers (e. g. 7σ).

We start by attempting to reproduce the results of [1, 2]. First we consider the 10-bin CMASSLOWZTOT-NGC results from [2] (top left in figure 2). We find $\chi^2 = 3399$ on the data, compared to a mean $\chi^2 = 2991$ and standard deviation of 144 on the mocks. The data has higher χ^2 by 2.84σ , or two-tailed p -value of 0.996 (equivalent to 2.9σ) by the non-parametric rank test, with 9 simulations having $\chi^2 > 3399$. Ref. [2] finds $\chi^2 = 3382$ on the data compared to $\chi^2 = 2999 \pm 162$ on the mocks, for a detection of 2.36σ or $p = 0.988$ (2.5σ) in the non-parametric rank test.¹⁸ The individual mock parity odd four-point correlation functions have $\chi^2 \equiv \Delta \hat{\mathcal{E}}_a (C_{\text{ana}}^{-1})^{ab} \Delta \hat{\mathcal{E}}_b \sim 60$, where $\Delta \hat{\mathcal{E}}_a$ is the change in parity-odd 4PCF between our work and [2]. Overall, the level of agreement with [2] is excellent.

Our baseline agreement with the 18-bin results of [1] is less good (bottom row of figure 2). Our baseline detection significance is 7.31σ for CMASS-NGC and 6.90σ for CMASSLOWZTOT-SGC, compared to 4.7σ in NGC and 5.4σ in SGC in [1]. Here, and throughout the paper when discussing the 18-bin case, we define the detection significance by dividing the difference in χ^2 by the standard deviation from the mocks; the non-parametric rank test from [2] is not useful because all mocks have χ^2 lower than the data.

Our reproduction of the 18-bin result is quite sensitive to various analysis choices. In

¹⁸Following the publicly available notebook in [https://github.com/oliverphilcox/Parity-Odd-4PCF/blob/main/BOSS%200dd-Parity%204PCF%20\(CS%20template\).ipynb](https://github.com/oliverphilcox/Parity-Odd-4PCF/blob/main/BOSS%200dd-Parity%204PCF%20(CS%20template).ipynb).

table 2, we summarize the detection significance of χ^2 under various analysis choices, also including the baseline choices.

If we instead use CMASSLOWZTOT-NGC and CMASS-SGC, we find detection significance of 5.35σ in NGC and 9.16σ in SGC. Hence, CMASS (7.31σ and 9.16σ) gives consistently higher detection significance than CMASSLOWZTOT (5.35σ and 6.90σ), driven by changes in χ_{data}^2 rather than changes in $\langle\chi_{\text{mock}}^2\rangle$. This suggests that the parity-odd four point detection is not driven by inhomogeneous sample selection issues in CMASSLOWZTOT, either created by the complex LOWZ selection function or an improper combination of CMASS and LOWZ with their slightly different angular weights and redshift distributions.

Our results also depend on the number density $\bar{n} = 1/P_0$ used to calculate the analytic covariance (table 1). Doubling the number density increases the CMASSLOWZTOT-SGC significance to 8.13σ whereas halving it decreases the significance to 5.50σ . This suggests that the detection is weighted towards small scales. Increasing the number density reduces shot noise and pushes the range of cosmic variance-limited modes to higher k , effectively up-weighting smaller scales.

The results are even slightly sensitive to the number of randoms used. If we double the number density of randoms on mocks and data, the significance decreases by 0.4σ . If we use the $50\times$ randoms on mocks, rather than randomly subsampling the $100\times$ randoms, the significance increases by 0.6σ . We measured these changes using the change in χ_{data}^2 and χ_{mock}^2 on 50 mocks; the scatter contributed by the limited number of mocks is therefore $1/\sqrt{50} = 0.15\sigma$.

Finally, we tested the impact of removing some of the weights applied to the data. The mocks do not have redshift failures and hence do not have w_{noz} . This leads to a significant difference in the tails of the distribution of $w_{\text{g,data}}$ and $w_{\text{g,mock}}$, and an even larger difference in the third and fourth moments of the weights $\langle w_{\text{g}}^3 \rangle$, $\langle w_{\text{g}}^4 \rangle$. Turning off w_{noz} in the data drops the CMASS-NGC detection significance from 7.32σ to 4.26σ .

Fiber collisions are added to the mocks in only an approximate way – and the impact of fiber collisions in the mocks is sensitive to the modeling of sub-Mpc scales, which does not match the data perfectly [20]. Turning off w_{cp} changes χ_{data}^2 substantially, from 22772 to 19747; it also substantially reduces $\langle\chi_{\text{mock}}^2\rangle$, from 19599 to 18344, and σ_{χ^2} , from 405 to 158. Thus, the detection significance goes up, from 7.3σ to 8.9σ , if we did not correct for fiber collisions in either the data or the mocks.

We also tried turning off the imaging systematics weights on data: again, the mocks do not have imaging systematics and hence do not have this weight, although turning off the weight will add an extra source of systematics in the data. In the 10-bin case, we find that this increases χ^2 from 3399 to 3581, increasing the detection significance from 2.65σ to 3.0σ .

Summarizing, we agree nearly perfectly with the 10-bin results from [2], and agree qualitatively with the 18-bin results from [1]. In the 18-bin case, the level of disagreement is comparable to the effect of varying analysis choices. This is good enough agreement that we are confident that we have reproduced the essential features of the analysis in [1, 2]. We find that the χ^2 detection significance remains high even after removing some of the systematics corrections from the data (though with $\sim 3\sigma$ changes), in agreement with the extensive set of validation tests in [1].

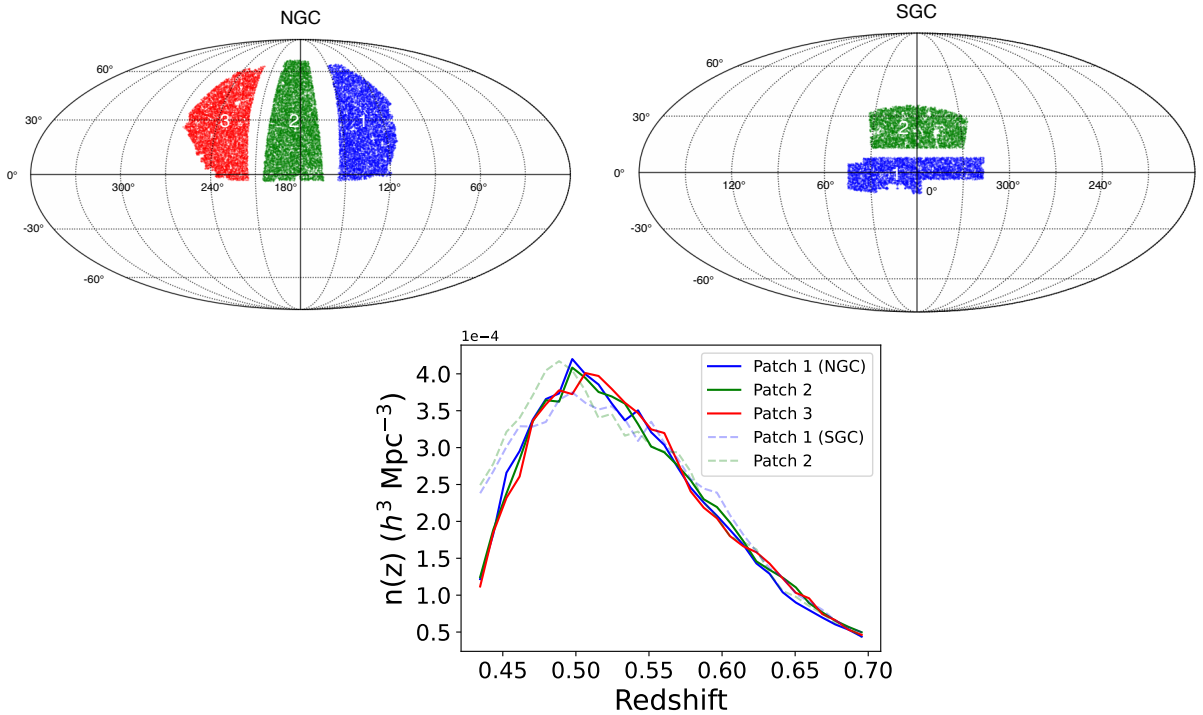


Figure 3. Patches considered for NGC (top left) and SGC (top right) to compute χ_x^2 and χ_{null}^2 . Note that the sky has been rotated between the NGC and SGC plots. Bottom panel shows the redshift distribution of all five patches, using the default choices, CMASS in the NGC and CMASSLOWZTOT in the SGC.

4 The new statistics χ_x^2 and χ_{null}^2

Throughout this section, we only consider the 18-bin case from [1] (rather than the 10-bin case from [2] – see section 3.1 for more discussion).

4.1 Splitting BOSS into patches

We divide each BOSS survey (either CMASS-NGC or CMASSLOWZTOT-SGC) into N_p patches, separated by 10° (5°) in the NGC (SGC) – corresponding to 140 (70) h^{-1} Mpc at $z = 0.4$ – in order to ensure statistical independence. We use $N_p = 3$ patches for CMASS-NGC, and $N_p = 2$ patches for CMASSLOWZTOT-SGC. The patches are defined with the following simple cuts in right ascension (RA) and declination (DEC), for NGC:

$$\begin{aligned}
 \text{RA} < 155^\circ - \frac{1}{12}\text{DEC} & && \text{(NGC patch 1)} \\
 165^\circ - \frac{1}{12}\text{DEC} < \text{RA} < 205^\circ - \frac{1}{12}\text{DEC} & && \text{(NGC patch 2)} \\
 215^\circ - \frac{1}{12}\text{DEC} < \text{RA} & && \text{(NGC patch 3)} \quad (4.1)
 \end{aligned}$$

and for SGC:

$$\begin{aligned}
 \text{DEC} < 8^\circ & && \text{(SGC patch 1)} \\
 \text{DEC} > 13^\circ & && \text{(SGC patch 2)} \quad (4.2)
 \end{aligned}$$

The sky and redshift distributions of the patches are shown in figure 3. The cuts remove 22% (12%) of the survey area in the NGC (SGC), respectively. The mean redshifts are $\bar{z} = 0.5417, 0.5477, 0.5475, 0.5461$ and 0.5424 for patches 1–3 in CMASS-NGC and patches 1–2 in CMASSLOWZTOT-SGC, respectively. The standard error of the mean is 0.00017 for the NGC patches and 0.00021 for the SGC patches, though since galaxies are correlated, the standard error of the mean underestimates the true error on \bar{z} as it neglects the cosmic variance contribution.

4.2 Definitions and notation

We use the term “survey” to mean either CMASS-NGC or CMASSLOWZTOT-SGC, the term “patch” to mean one of the patches $\mu = 1, \dots, N_p$ which comprise a survey, and the term “region” to mean either a survey or a patch.

We denote the parity-odd 4PCF for a survey by $\widehat{\mathcal{E}}_a$, and the parity-odd 4PCF for a patch by $\widehat{\mathcal{E}}_a^\mu$, where $\mu = 1, \dots, N_p$. We define the following covariance matrices:

$$(C_{\text{data}})_{ab} = \text{Covariance matrix } \langle \widehat{\mathcal{E}}_a \widehat{\mathcal{E}}_b \rangle \text{ of BOSS galaxy field (not directly observable)} \quad (4.3)$$

$$(C_{\text{mock}})_{ab} = \text{Covariance matrix } \langle \widehat{\mathcal{E}}_a \widehat{\mathcal{E}}_b \rangle \text{ of BOSS mocks (in the limit } N_{\text{mocks}} \rightarrow \infty) \quad (4.4)$$

$$(C_{\text{ana}})_{ab} = \text{Analytic covariance matrix from section 3.2} \quad (4.5)$$

In principle, C_{mock} could be computed by brute force with a large number of mocks ($N_{\text{mocks}} \gg N_{\text{dof}}$). In practice, we don’t have enough mocks, so we can’t estimate every entry of the dense matrix C_{mock} . (For example, this is why we define χ^2 as $\widehat{\mathcal{E}}_a (C_{\text{ana}}^{-1})^{ab} \widehat{\mathcal{E}}_b$ rather than $\widehat{\mathcal{E}}_a (C_{\text{mock}}^{-1})^{ab} \widehat{\mathcal{E}}_b$.)

Let $(C_{\text{mock}}^\mu)_{ab}$ and $(C_{\text{data}}^\mu)_{ab}$ denote the 4PCF covariance in a single patch (where $\mu = 1, \dots, N_p$). We expect the covariance to scale with survey volume roughly as $1/V$, so a single-patch covariance C_{ab}^μ will be larger than the corresponding full-survey covariance C_{ab} . To quantify this, we define the “effective volume” V_{eff} of the full survey and each patch μ by:

$$V_{\text{eff}} \equiv \frac{V_{\text{fid}} N_{\text{dof}}}{\text{Tr}(C_{\text{ana}}^{-1} C_{\text{mock}})} \quad V_{\text{eff}}^\mu \equiv \frac{V_{\text{fid}} N_{\text{dof}}}{\text{Tr}(C_{\text{ana}}^{-1} C_{\text{mock}}^\mu)} \quad (4.6)$$

The traces in the denominators can be computed by Monte Carlo, e.g. $\text{Tr}(C_{\text{ana}}^{-1} C_{\text{mock}}) = \langle \widehat{\mathcal{E}}_a (C_{\text{ana}}^{-1})^{ab} \widehat{\mathcal{E}}_b \rangle_{\text{mock}}$. In table 3, we show values of $V_{\text{eff}}, V_{\text{eff}}^\mu$ computed using this method.

We assume that $\widehat{\mathcal{E}}_a$ is an unbiased estimator of \mathcal{E}_a (the true parity-odd four-point function of the universe):

$$\langle \widehat{\mathcal{E}}_a \rangle_{\text{data}} = \bar{\mathcal{E}}_a \quad \langle \widehat{\mathcal{E}}_a \rangle_{\text{mock}} = 0 \quad (4.7)$$

Then, by definition of C_{data} and C_{mock} , we have:

$$\langle \widehat{\mathcal{E}}_a \widehat{\mathcal{E}}_b \rangle_{\text{data}} = \bar{\mathcal{E}}_a \bar{\mathcal{E}}_b + (C_{\text{data}})_{ab} \quad \langle \widehat{\mathcal{E}}_a \widehat{\mathcal{E}}_b \rangle_{\text{mock}} = (C_{\text{mock}})_{ab} \quad (4.8)$$

In section 1, we stated without proof that the quantity $\langle \chi^2 \rangle_{\text{data}} - \langle \chi^2 \rangle_{\text{mock}}$ (i.e. the “excess” χ^2) was the sum of parity violation and data–mock mismatch terms (eq. (1.7)). Now we can prove this formally as follows:

$$\begin{aligned} \langle \chi^2 \rangle_{\text{data}} - \langle \chi^2 \rangle_{\text{mock}} &= \langle \widehat{\mathcal{E}}_a (C_{\text{ana}}^{-1})^{ab} \widehat{\mathcal{E}}_b \rangle_{\text{data}} - \langle \widehat{\mathcal{E}}_a (C_{\text{ana}}^{-1})^{ab} \widehat{\mathcal{E}}_b \rangle_{\text{mock}} \\ &= (C_{\text{ana}}^{-1})^{ab} (\bar{\mathcal{E}}_a \bar{\mathcal{E}}_b + (C_{\text{data}})_{ab}) - (C_{\text{ana}}^{-1})^{ab} (C_{\text{mock}})_{ab} \\ &= \underbrace{\bar{\mathcal{E}}_a (C_{\text{ana}}^{-1})^{ab} \bar{\mathcal{E}}_b}_{\text{parity violation}} + \underbrace{\text{Tr}[(C_{\text{data}} - C_{\text{mock}}) C_{\text{ana}}^{-1}]}_{\text{data–mock mismatch}} \end{aligned} \quad (4.9)$$

In the first line, we used the definition (3.10) of χ^2 , and in the second line we used eq. (4.8).

Region	Effective volume
CMASS-NGC	
Full survey	$V_{\text{eff}} = 2.37 h^{-3} \text{ Gpc}^3$
Patch $\mu = 1$	$V_{\text{eff}}^\mu = 0.52 h^{-3} \text{ Gpc}^3$
Patch $\mu = 2$	$V_{\text{eff}}^\mu = 0.58 h^{-3} \text{ Gpc}^3$
Patch $\mu = 3$	$V_{\text{eff}}^\mu = 0.53 h^{-3} \text{ Gpc}^3$
CMASSLOWZTOT-SGC	
Full survey	$V_{\text{eff}} = 0.76 h^{-3} \text{ Gpc}^3$
Patch $\mu = 1$	$V_{\text{eff}}^\mu = 0.29 h^{-3} \text{ Gpc}^3$
Patch $\mu = 2$	$V_{\text{eff}}^\mu = 0.30 h^{-3} \text{ Gpc}^3$

Table 3. Effective volumes V_{eff} and V_{eff}^μ defined in eq. (4.6).

4.3 The statistic χ_\times^2

We define the new statistic χ_\times^2 by:

$$\chi_\times^2 \equiv \frac{1}{N_p(N_p - 1)} \sum_{\mu \neq \nu} \hat{\mathcal{E}}_a^\mu (C_{\text{ana}}^{-1})^{ab} \hat{\mathcal{E}}_b^\nu \quad (4.10)$$

In section 1, we argued that χ_\times^2 is sensitive to parity violation but not data–mock mismatch. Intuitively, this is because χ_\times^2 is constructed from cross-correlations between patches, and cross-correlations are not sensitive to data–mock mismatch (which acts as “noise” which is uncorrelated between patches). We will prove this formally shortly, but first we want to state our assumptions explicitly:

- *Assumption 1.* When we estimate the parity-odd 4PCF in a single patch, rather than a full survey, the estimator $\hat{\mathcal{E}}_a^\mu$ is still unbiased:

$$\langle \hat{\mathcal{E}}_a^\mu \rangle_{\text{data}} = \bar{\mathcal{E}}_a \quad \langle \hat{\mathcal{E}}_a^\mu \rangle_{\text{mock}} = 0 \quad (4.11)$$

(Note that this equation is the same as eq. (4.7), but with a μ index added.)

- *Assumption 2.* For patches $\mu \neq \nu$, the estimators $\hat{\mathcal{E}}_a^\mu$ and $\hat{\mathcal{E}}_b^\nu$ are uncorrelated:

$$\langle \hat{\mathcal{E}}_a^\mu \hat{\mathcal{E}}_b^\nu \rangle_{\text{data}} = \bar{\mathcal{E}}_a \bar{\mathcal{E}}_b + (C_{\text{data}}^\mu)_{ab} \delta^{\mu\nu} \quad \langle \hat{\mathcal{E}}_a^\mu \hat{\mathcal{E}}_b^\nu \rangle_{\text{mock}} = (C_{\text{mock}}^\mu)_{ab} \delta^{\mu\nu} \quad (4.12)$$

where the $\delta^{\mu\nu}$ factors follow from the assumption of uncorrelated patches, and the rest of eq. (4.12) follows from eq. (4.11) and the definitions of C_{data}^μ and C_{mock}^μ . (Note the similarity between eqs. (4.8) and (4.12).)

As a test of assumption 2, we verified that for each patch pair $\mu \neq \nu$, the quantity $\langle \hat{\mathcal{E}}_a^\mu (C_{\text{ana}}^{-1})^{ab} \hat{\mathcal{E}}_b^\nu \rangle_{\text{mock}}$ is zero, within statistical errors from the finite number of mocks. (If the spatial “padding” between sky patches in figure 3 were reduced, we expect that this test would eventually fail.)

Now we give a formal proof that χ_{\times}^2 is sensitive to parity violation but not data–mock mismatch, by computing $\langle \chi_{\times}^2 \rangle_{\text{data}}$ as follows:

$$\begin{aligned}
\langle \chi_{\times}^2 \rangle_{\text{data}} &= \frac{1}{N_p(N_p - 1)} \sum_{\mu \neq \nu} (C_{\text{ana}}^{-1})^{ab} \langle \widehat{\mathcal{E}}_a^\mu \widehat{\mathcal{E}}_b^\nu \rangle && \text{using definition (4.10) of } \chi_{\times}^2 \\
&= \frac{1}{N_p(N_p - 1)} \sum_{\mu \neq \nu} (C_{\text{ana}}^{-1})^{ab} \bar{\mathcal{E}}_a \bar{\mathcal{E}}_b && \text{by eq. (4.12)} \\
&= \underbrace{\bar{\mathcal{E}}_a (C_{\text{ana}}^{-1})^{ab} \bar{\mathcal{E}}_b}_{\text{parity violation}} && (4.13)
\end{aligned}$$

As expected, we get the same parity violation term as in our previous calculation (4.9) of $\langle \chi^2 \rangle$, but without the data–mock mismatch term. (As a check, we note that a similar calculation predicts $\langle \chi_{\times}^2 \rangle_{\text{mock}} = 0$. We checked that this prediction is satisfied, within statistical errors due to the finite number of mocks.)

In the top panels of figure 4, we evaluate χ_{\times}^2 on BOSS data. The result is consistent with zero (at 1.8σ and 1.7σ , for CMASS-NGC and CMASSLOWZTOT-SGC respectively), as would be expected if the 7σ excess χ^2 (seen previously in figure 2) were due to data–mock mismatch. The purple lines in the top panels also show the value of χ_{\times}^2 that would be expected if the previously-seen excess χ^2 were due entirely to parity violation:

$$(\text{Parity violation expectation for } \chi_{\times}^2) = \chi_{\text{data}}^2 - \langle \chi^2 \rangle_{\text{mock}} \quad (4.14)$$

These values of χ_{\times}^2 are inconsistent with the data, at 5.9σ and 9.4σ for CMASS-NGC and CMASSLOWZTOT-SGC respectively. This shows that the 7σ excess χ^2 (figure 2) cannot be entirely (or even mostly) due to parity violation – there must be contributions due to data–mock mismatch or systematics. We emphasize that this conclusion only depends on assumptions 1 and 2 above, which are quite minimal.

One interesting detail: for both CMASS-NGC and CMASSLOWZTOT-SGC, we have $\text{Var}(\chi_{\times}^2) < \text{Var}(\chi^2)$. That is, the estimator χ_{\times}^2 is both more robust than χ^2 (since there is no bias from data–mock mismatch), and more statistically optimal. This phenomenon surprised us initially, but after some exploration we concluded that it is a finite-volume effect (and the inequality would be reversed for a survey which is larger than BOSS). We explain this in detail in appendix B.

4.4 The statistic χ_{null}^2

The χ_{\times}^2 results from the previous section are sufficient to conclude that there is no compelling evidence for parity violation in BOSS. However, for the sake of completeness and pedagogy, we can also define a statistic χ_{null}^2 which is sensitive to data–mock mismatch but not parity violation:

$$\chi_{\text{null}}^2 \equiv \frac{1}{\mathcal{N}} \sum_{\mu \neq \nu} (\widehat{\mathcal{E}}_a^\mu - \widehat{\mathcal{E}}_a^\nu) (C_{\text{ana}}^{-1})^{ab} (\widehat{\mathcal{E}}_b^\mu - \widehat{\mathcal{E}}_b^\nu) \quad (4.15)$$

where the normalization \mathcal{N} is defined by:

$$\mathcal{N} \equiv 2(N_p - 1) \sum_{\mu} \frac{V_{\text{eff}}}{V_{\text{eff}}^{\mu}} \quad (4.16)$$

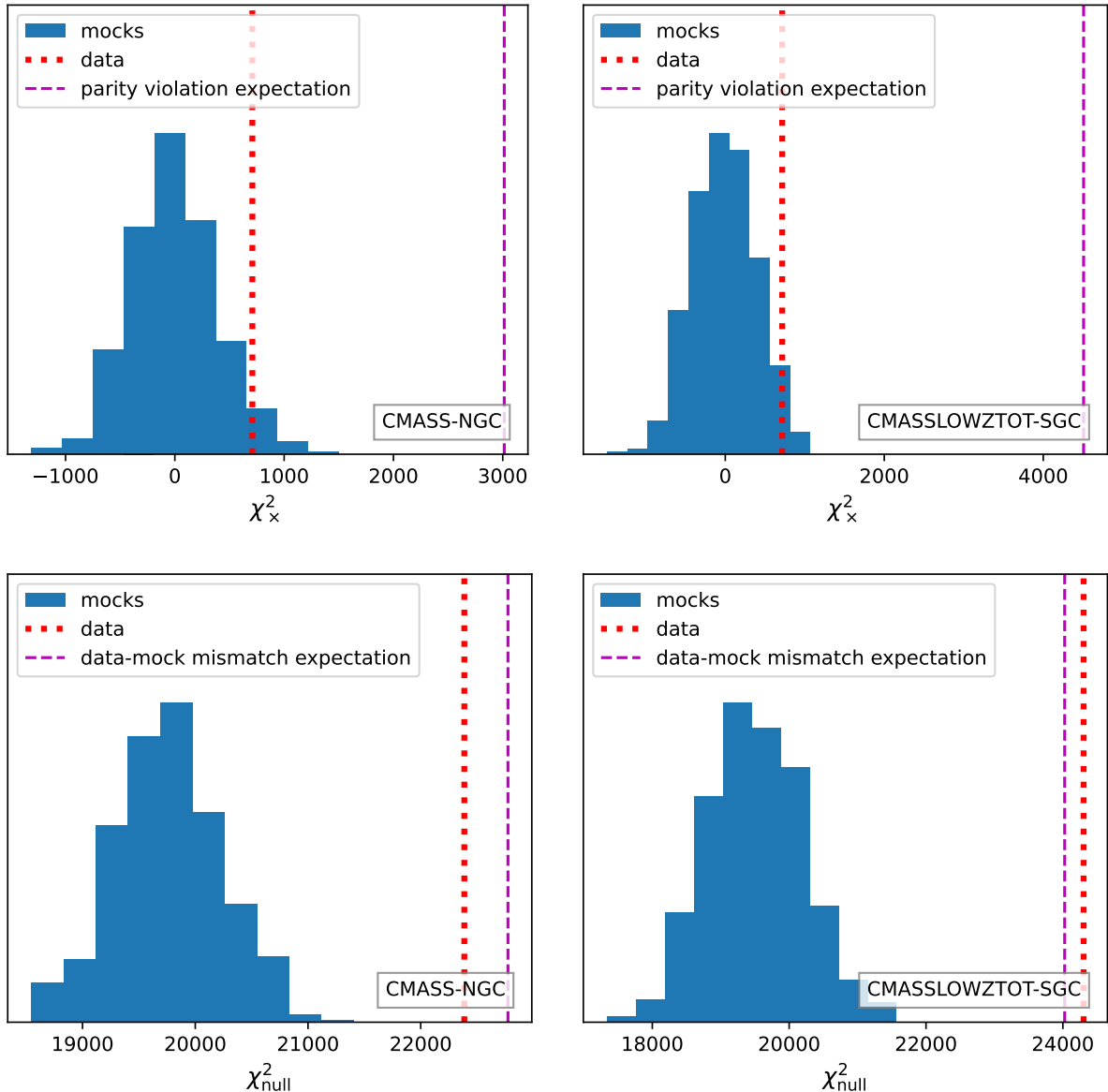


Figure 4. *Top row.* The statistic χ_x^2 evaluated on mocks (histograms) and data (dotted lines). The values of χ_x^2 are consistent with zero, as expected if the $\sim 7\sigma$ signal in figure 2 were due to data–mock mismatch. We also show (dashed lines) the “parity violation expectation”, i. e. expected value of χ_x^2 if the $\sim 7\sigma$ signal were due to parity violation (eq. (4.14)). These values of χ_x^2 are ruled out at 5.9σ and 9.4σ for CMASS-NGC (left) and CMASSLOWZTOT-SGC (right). ***Bottom row.*** The statistic χ_{null}^2 evaluated on mocks (histogram) and data (dotted lines). The data is inconsistent with mocks, indicating null test failure and evidence for data–mock mismatch. We also show (dashed lines) the “data–mock mismatch expectation”, i. e. expected value of χ_{null}^2 if the $\sim 7\sigma$ signal in figure 2 were due to data–mock mismatch (eq. (4.22)). The data is consistent with these values, within statistical errors from the mocks.

The full-survey effective volume V_{eff} and single-patch effective volume V_{eff}^μ were defined in eq. (4.6).

In section 1, we argued that χ_{null}^2 is sensitive to data–mock mismatch but not parity violation. Intuitively, this is because χ_{null}^2 defines a null test: it measures consistency between the four-point function in different parts of the sky. Parity violation (i.e. $\bar{\mathcal{E}}_a \neq 0$) does not contribute to χ_{null}^2 , since we still expect consistent values of $\hat{\mathcal{E}}_a$ in different parts of the sky.

To show this formally, we compute $\langle \chi_{\text{null}}^2 \rangle_{\text{data}}$ as follows:

$$\begin{aligned} \langle \chi_{\text{null}}^2 \rangle_{\text{data}} &= \frac{1}{\mathcal{N}} \sum_{\mu \neq \nu} \left\langle (\hat{\mathcal{E}}_a^\mu - \hat{\mathcal{E}}_a^\nu) (C_{\text{ana}}^{-1})^{ab} (\hat{\mathcal{E}}_b^\mu - \hat{\mathcal{E}}_b^\nu) \right\rangle_{\text{data}} && \text{using definition (4.15) of } \chi_{\text{null}}^2 \\ &= \frac{1}{\mathcal{N}} \sum_{\mu \neq \nu} (C_{\text{ana}}^{-1})^{ab} (C_{\text{data}}^\mu + C_{\text{data}}^\nu)_{ab} && \text{using eq. (4.12)} \\ &= \frac{2(N_p - 1)}{\mathcal{N}} \sum_{\mu} \text{Tr}(C_{\text{ana}}^{-1} C_{\text{data}}^\mu) \end{aligned} \quad (4.17)$$

Similarly, we have $\langle \chi_{\text{null}}^2 \rangle_{\text{mock}} = 2\mathcal{N}^{-1}(N_p - 1) \sum_{\mu} \text{Tr}(C_{\text{ana}}^{-1} C_{\text{mock}}^\mu)$, and therefore:

$$\langle \chi_{\text{null}}^2 \rangle_{\text{data}} - \langle \chi_{\text{null}}^2 \rangle_{\text{mock}} = \frac{2(N_p - 1)}{\mathcal{N}} \sum_{\mu} \text{Tr}[(C_{\text{data}}^\mu - C_{\text{mock}}^\mu) C_{\text{ana}}^{-1}] \quad (4.18)$$

which shows that χ_{null}^2 is sensitive to data–mock mismatch ($C_{\text{data}}^\mu \neq C_{\text{mock}}^\mu$) but not parity violation ($\bar{\mathcal{E}}_a \neq 0$).

In the bottom panels of figure 4, we evaluate χ_{null}^2 on BOSS. The values are not statistically consistent with mocks, indicating null test failure and unambiguous evidence for data–mock mismatch (or systematics), at 5.6σ (6.8σ) for CMASS-NGC (CMASSLOWZTOT-SGC).¹⁹

We emphasize that our results so far only depend on assumptions 1 and 2 (i.e. $\hat{\mathcal{E}}_a^\mu$ is unbiased, and patches $\mu \neq \nu$ are uncorrelated). In order to assign a normalization to χ_{null}^2 and interpret its numerical value, we add a more technical assumption:

- *Assumption 3.* The single-patch covariance matrices $C_{\text{data}}^\mu, C_{\text{mock}}^\mu$ are approximately proportional to their full-survey counterparts $C_{\text{data}}, C_{\text{mock}}$.

This assumption implies the apparently stronger identity:

$$C_{\text{data}}^\mu \approx \frac{V_{\text{eff}}}{V_{\text{eff}}^\mu} C_{\text{data}} \quad C_{\text{mock}}^\mu \approx \frac{V_{\text{eff}}}{V_{\text{eff}}^\mu} C_{\text{mock}} \quad (4.19)$$

by the following argument. Suppose that C_{data}^μ and C_{data} are proportional, i.e. $C_{\text{data}}^\mu = AC_{\text{data}}$. Multiplying both sides by C_{ana}^{-1} and taking traces, we get:

$$A = \frac{\text{Tr}(C_{\text{ana}}^{-1} C_{\text{data}}^\mu)}{\text{Tr}(C_{\text{ana}}^{-1} C_{\text{data}})} = \frac{V_{\text{eff}}}{V_{\text{eff}}^\mu} \quad (4.20)$$

¹⁹We also find that the per-patch χ^2 statistic $\hat{\mathcal{E}}_a^\mu (C_{\text{ana}}^{-1})^{ab} \hat{\mathcal{E}}_b^\mu$ fluctuates between patches: we get 4.0σ in NGC patch 1, 1.8σ in NGC patch 2, 4.4σ in NGC patch 3, 2.2σ in SGC patch 1, and 8.2σ in SGC patch 2. This is a different null test than χ_{null}^2 , since it compares 8PCFs between patches rather than 4PCFs.

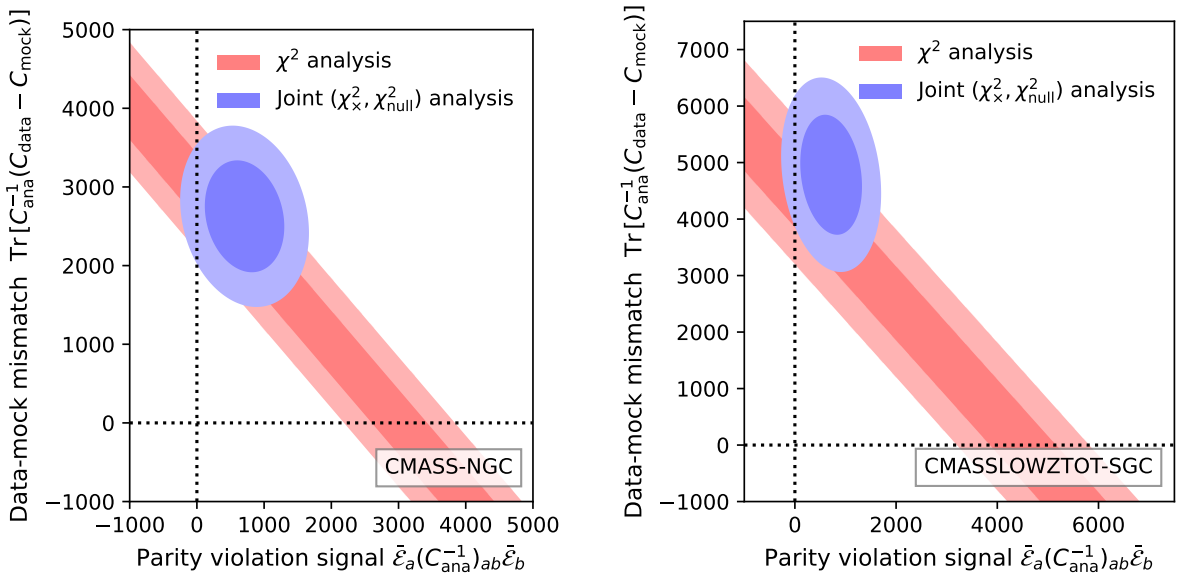


Figure 5. Summary plots combining previous results from figures 2 and 4. The horizontal (x) and vertical (y) axes represent the parity violation signal $x = \hat{\mathcal{E}}_a(C_{\text{ana}}^{-1})^{ab}\hat{\mathcal{E}}_b$, and the data–mock mismatch $y = \text{Tr}[(C_{\text{data}} - C_{\text{mock}})C_{\text{ana}}^{-1}]$, respectively. The statistics χ^2 , χ_x^2 , and χ_{null}^2 measure the parameter combinations $(x + y)$, x , and y . The red regions correspond to the χ^2 -analysis in figure 2 and are consistent with either parity violation or data–mock mismatch. The blue regions combine χ_x^2 and χ_{null}^2 results from figure 4, and show consistency with data–mock mismatch, with no statistically significant evidence for parity violation. Throughout this plot, statistical errors are assumed Gaussian, with covariance estimated from mock catalogs. Light/dark regions are 68 % and 95 % CL.

This proves the first half of eq. (4.19). The second half follows by the same argument (replacing $(\cdot)_{\text{data}}$ by $(\cdot)_{\text{mock}}$ everywhere). Next, plugging eq. (4.19) into eq. (4.18), we get:

$$\langle \chi_{\text{null}}^2 \rangle_{\text{data}} - \langle \chi_{\text{null}}^2 \rangle_{\text{mock}} = \underbrace{\text{Tr}[(C_{\text{data}} - C_{\text{mock}})C_{\text{ana}}^{-1}]}_{\text{data–mock mismatch}} \quad (4.21)$$

i. e. the data–mock mismatch term is the same as in our previous calculation (4.9) of $\langle \chi^2 \rangle$, but without the parity violation term.

Now we can answer the sharper question: is the numerical value of χ_{null}^2 consistent with the statement that the $\sim 7\sigma$ χ^2 excess from figure 2 is entirely due to data–mock mismatch? To answer this, we compare χ_{null}^2 with its “data–mock mismatch expectation”:

$$(\text{Data–mock mismatch expectation for } \chi_{\text{null}}^2) = \langle \chi_{\text{null}}^2 \rangle_{\text{mock}} + \underbrace{(\chi_{\text{data}}^2 - \langle \chi^2 \rangle_{\text{mock}})}_{\text{Excess } \chi^2 \text{ from figure 2}} \quad (4.22)$$

In the bottom panel of figure 4, we show that χ_{null}^2 is statistically consistent with the data–mock mismatch expectation defined by eq. (4.22). This is expected if the $\sim 7\sigma$ χ^2 excess from figure 2 were entirely due to data–mock mismatch.

Finally, in figure 5, we combine our previous results from figures 2 and 4 into two summary plots, for CMASS-NGC and CMASSLOWZTOT-SGC. Each statistic considered so far (χ^2 , χ_x^2 , and χ_{null}^2) can be interpreted as measuring the parity violation signal $\hat{\mathcal{E}}_a(C_{\text{ana}}^{-1})^{ab}\hat{\mathcal{E}}_b$

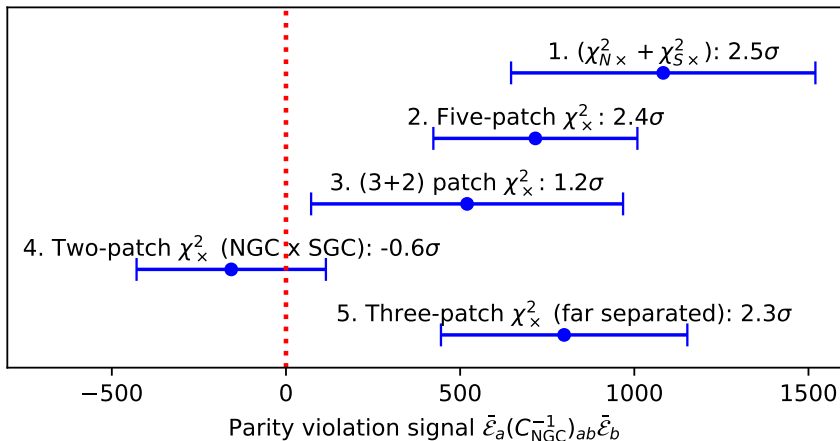


Figure 6. Statistical significance of parity violation when combining the NGC and SGC, obtained from five different summary statistics (see descriptions in section 4.5). In order to combine all five statistics in the same plot, we normalize each statistic so that its expectation value is $\bar{\epsilon}_a C_{\text{NGC}}^{-1} \bar{\epsilon}_b$, where C_{NGC} is the 18-bin NGC analytic covariance (see table 1).

on the horizontal axis, and/or the data–mock mismatch $\text{Tr}[(C_{\text{data}} - C_{\text{mock}})C_{\text{ana}}^{-1}]$ on the vertical axis. An analysis based only on the χ^2 statistic shows that the sum of the two signals is nonzero at $\sim 7\sigma$ (red regions). A joint analysis based on the χ_{x}^2 and χ_{null}^2 statistics separates the two signals. The joint analysis shows no statistically significant evidence for parity violation (blue regions).

4.5 Combined NGC + SGC significance

In this section we address the question, “what is the global significance of parity violation, combining NGC and SGC”? In particular, since χ_{x}^2 is nonzero at 1.8σ in the NGC and 1.7σ in the SGC (section 4.3), one may wonder whether the global significance is $(1.8 + 1.7)/\sqrt{2} = 2.5\sigma$.

In order to assign global significance, we must choose a summary statistic. We find that different, well-motivated summary statistics give different results. In figure 6, we compare five summary statistics as follows (from top to bottom):

1. $(\chi_{\text{NGC}}^2 + \chi_{\text{SGC}}^2)$: This summary statistic is defined by simply adding the χ_{x}^2 statistics in the NGC and SGC.
2. Five-patch χ_{x}^2 : This statistic is defined by treating the three NGC patches and the two SGC patches (see figure 3) as a single survey with $N_p = 5$, and then defining χ_{x}^2 as usual (eq. (4.10)).
3. (3+2)-patch χ_{x}^2 : This statistic is defined similarly to χ_{x}^2 , by summing over all (3×2) pairs of the form (NGC patch) \times (SGC patch).
4. Two-patch χ_{x}^2 (NGC \times SGC): this statistic is defined by treating the entire NGC as a single patch, and the entire SGC as a second patch, then defining χ_{x}^2 as usual (eq. (4.10)) with $N_p = 2$. (Statistics #3 and #4 are conceptually similar, but non-identical due to edge effects.)

5. Three-patch χ_{\times}^2 (far separated): This statistic is defined by taking the two most separated patches in the NGC (see figure 3), and treating the entire SGC as a third patch, then defining χ_{\times}^2 as usual with $N_p = 3$.²⁰

Throughout figure 6, we assign error bars by evaluating the same summary statistic (e.g. $(\chi_{\text{N}\times}^2 + \chi_{\text{S}\times}^2)$ for the top error bar) on both data and mocks. (In all cases, the mean value of the summary statistic in mocks is consistent with zero, as expected since the mocks are parity-invariant.)

Since summary statistics 1–5 are derived from the same catalogs, they are correlated, and there is more statistical tension in figure 6 than the error bars would suggest. In particular, the discrepancy between summary statistic #4 (which has the smallest error bar), and summary statistic #2 (which is a close second) is 3.1σ relative to mocks.

It is unclear why there is significant tension in figure 6 relative to mocks. It may be a symptom of undiagnosed systematics (especially systematics related to LSS weights $w_{\text{noz}}, w_{\text{cp}}, w_{\text{sys}}$, see discussion in section 3.3). Another possible explanation of the tension in figure 6 is that error bars have been systematically underestimated, as we now explain in more detail.

The χ_{\times}^2 statistic has been constructed so that data–mock mismatch does not contribute to $\langle \chi_{\times}^2 \rangle$. However, we still use mocks to estimate the *variance* of χ_{\times}^2 . Therefore, data–mock mismatch can still produce a small *multiplicative* bias to $\text{Var}(\chi_{\times}^2)$. More quantitatively, it is plausible that we are underestimating error bars on χ_{\times}^2 by $\sim 20\%$ throughout the paper, since the results of this paper suggest that the mocks underestimate the 4PCF covariance C_{ab} by 20% (section 1). This is much less serious than the original χ^2 statistic, where data–mock mismatch can produce a large *additive bias*, e.g. a null result could appear to be a 7σ excess in χ^2 .

Nevertheless, the issue of underestimating error bars complicates the interpretation of the NGC+SGC results in figure 6. The NGC+SGC significance varies between (-0.6σ) and 2.5σ , depending on which summary statistic is used, and the level of tension between summary statistics can be as large as 3.1σ . Given this level of discrepancy and tension, and the possibility of underestimating error bars, our interpretation of figure 6 is that there is not compelling evidence for parity violation when combining the NGC and SGC.

5 Discussion

The main results of this paper can be summarized as follows:

- The χ^2 statistic introduced in [1, 2] shows a $\sim 7\sigma$ excess in BOSS (figure 2). However, we show in eq. (4.9) that $\langle \chi^2 \rangle$ contains two terms: a parity violation term, and a “data–mock mismatch” term. The data–mock mismatch term is nonzero if the *parity-even* 8PCF of the mocks does not match the data (which leads to a biased estimate of the parity-odd 4PCF covariance). We define new statistics χ_{\times}^2 and χ_{null}^2 (eqs. (4.10) and (4.15)) which separate the two terms.

²⁰Since summary statistics 1–5 depend on a choice of C_{ana} , there is a potential ambiguity since one may choose to use either $C_{\text{ana}}^{\text{NGC}}$ or $C_{\text{ana}}^{\text{SGC}}$. However, in the 18-bin case, our covariance matrices $C_{\text{ana}}^{\text{NGC}}$ and $C_{\text{ana}}^{\text{SGC}}$ are proportional, since the two surveys have the same P_0 but different V_{fid} (table 1). Therefore, the only ambiguity is the overall normalization of the summary statistic. We have chosen to normalize all five summary statistics to have expectation value $\bar{\mathcal{E}}_a C_{\text{NGC}}^{-1} \bar{\mathcal{E}}_b$, so that they can be compared to each other in figure 6.

- The χ_x^2 statistic is an improved version of χ^2 which is both **more robust** and **more statistically optimal**. It is more robust in the sense that χ_x^2 is sensitive only to parity violation, with no bias from data–mock mismatch (eq. (4.13)). It is more statistically optimal in the sense that $\text{Var}(\chi_x^2) \lesssim \text{Var}(\chi^2)$ (due to a finite-volume effect, see appendix B).

When χ_x^2 is applied to the NGC or SGC separately, the result is statistically consistent with zero (figure 4, top row). This **rules out parity violation** (at 5.9σ and 9.4σ for CMASS-NGC and CMASSLOWZTOT-SGC) as the explanation for the $\sim 7\sigma$ excess χ^2 from the previous bullet point.

- Conversely, the χ_{null}^2 statistic defines a null test which is not sensitive to parity violation, but is sensitive to data–mock mismatch (eq. (4.18)). If we apply χ_{null}^2 to BOSS data, we get a statistically significant excess χ_{null}^2 (figure 4 bottom row), at 5.6σ (6.8σ) for CMASS-NGC (CMASSLOWZTOT-SGC). This is a **failing null test which implies data–mock mismatch (or systematics) with high statistical significance**.
- The previous results have made minimal assumptions: the per-patch estimator $\widehat{\mathcal{E}}_a^\mu$ is unbiased, and patches $\mu \neq \nu$ are uncorrelated (“Assumptions 1 and 2” in section 4.4). Assumption 2 predicts that $\langle \chi_x^2 \rangle = 0$; we have found this to be true on the mocks within the error expected from the finite number of mocks. If we add the technical assumption that single-patch covariances are proportional to full-survey covariances (“Assumption 3” in section 4.4), then we pin down the normalization of χ_{null}^2 .

When we do this (section 4.4 and figure 5), we find that the χ^2 excess from the first bullet point is equal (within statistical errors) to the χ_{null}^2 excess (which is sensitive to data–mock mismatch but not parity violation). This **further supports the hypothesis that the 7σ χ^2 excess is due to data–mock mismatch**.

- Most results in the paper treat the NGC and SGC separately. In section 4.5 we consider the combined NGC+SGC statistical significance. We find that different, well-motivated summary statistics give statistical significances between (-0.6σ) and 2.5σ , and the statistical tension between summary statistics (relative to mocks) can be as high as 3.1σ .

Given the level of discrepancy and tension between summary statistics, our interpretation is that there is **not compelling evidence for parity violation when combining the NGC and SGC**. We speculate that the tension is due to either undiagnosed systematics, or underestimating error bars (section 4.5).

These results are consistent with the results of [1, 2] being due to data–mock mismatch, rather than parity violation. This does not imply that there are parity-odd systematics in BOSS – it would suffice to have a $\sim 20\%$ difference between the parity-even 8PCF of the mocks and data. Such a difference is plausible since the mocks are primarily intended to model the large-scale 2PCF [20, 21].

One issue throughout our analysis is that we still use mocks to estimate the *variance* of our new statistic χ_x^2 . In section 4.5 we argue that error bars on χ_x^2 could plausibly be underestimated by $\sim 20\%$ throughout the paper. This complicates the interpretation of results with borderline statistical significance (say 2 – 2.5σ), such as the combined NGC+SGC results in section 4.5. In future work, it would be interesting to find a better way to assign error bars, e.g. removing dependence on mocks entirely by estimating $\text{Var}(\chi_x^2)$ directly from

data using a jackknife procedure (see [39] for some interesting recent suggestions along these lines).

An extended technical comment on patches. Since we have defined $\chi_{\times}^2, \chi_{\text{null}}^2$ by splitting the survey into patches, our results will depend on the number and choice of patches. If needed, we speculate that χ_{\times}^2 could be defined in a “patch-free” way, which we sketch as follows. We “promote” the estimator $\widehat{\mathcal{E}}_a$ to a 3D field $\widehat{\mathcal{E}}_a(\mathbf{x})$ by removing the outer integral $\int d^3\mathbf{x} \dots$ in (eq. (3.3)):

$$\widehat{\mathcal{E}}_{l_1 l_2 l_3}^{\beta_1 \beta_2 \beta_3}(\mathbf{x}) \equiv (-1)^{\sum l_i} \sum_{m_1 m_2 m_3} \begin{pmatrix} l_1 & l_2 & l_3 \\ m_1 & m_2 & m_3 \end{pmatrix} \delta_{\mathbf{g}}(\mathbf{x}) \left(\prod_{i=1}^3 \int d^3\mathbf{r}_i W_{l_i m_i}^{\beta_i}(\mathbf{r}_i) \delta_{\mathbf{g}}(\mathbf{x} + \mathbf{r}_i) \right) \quad (5.1)$$

and we “promote” the estimator χ^2 to a correlation function $\chi^2(\mathbf{r})$:

$$\chi^2(\mathbf{r}) \equiv \frac{1}{V_{\text{fid}}} \int d^3\mathbf{x} \widehat{\mathcal{E}}_a(\mathbf{x}) (C_{\text{ana}}^{-1})^{ab} \widehat{\mathcal{E}}_b(\mathbf{x} + \mathbf{r}) \quad (5.2)$$

In this notation, the original χ^2 statistic is $V_{\text{fid}}^{-1} \int d^3\mathbf{r} \chi^2(\mathbf{r})$. We can define an alternate statistic χ_{far}^2 by restricting the integral to large separations (say $|\mathbf{r}| > 100$ Mpc). This is roughly equivalent to splitting the survey into a large number of small patches, and constructing a χ_{\times}^2 -type statistic by cross-correlating patch pairs whose separation is large. Therefore, χ_{far}^2 should be sensitive to parity violation but not data–mock mismatch (like χ_{\times}^2 , but without choosing patches explicitly). We defer exploration of χ_{far}^2 to future work. (Adapting the edge correction procedure from [1, 2] to χ_{far}^2 may be nontrivial.)

Despite this null result for parity violation in BOSS, it will be interesting to search for parity violation in future datasets such as DESI [17]. The χ^2 statistic from [1, 2] has the advantage of being template-free (i. e. no specific model for the parity-odd 4PCF is assumed), but the disadvantage of being biased by data–mock mismatch. Therefore, any “detection” of parity violation based on χ^2 alone seems likely to remain inconclusive – parity violation and data–mock mismatch would both be plausible explanations. In this paper, we have constructed new statistics $\chi_{\times}^2, \chi_{\text{null}}^2$ which separate parity violation from data–mock mismatch, leading to an unambiguous conclusion.

Acknowledgments

AK, SM and KMS have contributed equally to this work and are listed alphabetically in the author list. We thank the authors of [1, 2] for making so much of their code publicly available, and for giving many useful comments on the draft. We particularly thank Jiamin Hou for sharing the analytic covariance code for the parity-odd four-point function. AK was supported as a CITA National Fellow by the Natural Sciences and Engineering Research Council of Canada (NSERC), funding reference #DIS-2022-568580. SM acknowledges support by the National Science Foundation under Grant No. 2108931. KMS was supported by an NSERC Discovery Grant, by the Daniel Family Foundation, and by the Centre for the Universe at Perimeter Institute. Research at Perimeter Institute is supported by the Government of Canada through Industry Canada and by the Province of Ontario through the Ministry of Research & Innovation.

References

- [1] J. Hou, Z. Slepian and R.N. Cahn, *Measurement of Parity-Odd Modes in the Large-Scale 4-Point Correlation Function of SDSS BOSS DR12 CMASS and LOWZ Galaxies*, [arXiv:2206.03625](#).
- [2] O.H.E. Philcox, *Probing parity violation with the four-point correlation function of BOSS galaxies*, *Phys. Rev. D* **106** (2022) 063501 [[arXiv:2206.04227](#)].
- [3] R.N. Cahn, Z. Slepian and J. Hou, *Test for Cosmological Parity Violation Using the 3D Distribution of Galaxies*, *Phys. Rev. Lett.* **130** (2023) 201002 [[2110.12004](#)].
- [4] J. Hou, R.N. Cahn, O.H.E. Philcox and Z. Slepian, *Analytic Gaussian covariance matrices for galaxy N-point correlation functions*, *Phys. Rev. D* **106** (2022) 043515 [[arXiv:2108.01714](#)].
- [5] G. Cabass, S. Jazayeri, E. Pajer and D. Stefanyszyn, *Parity violation in the scalar trispectrum: no-go theorems and yes-go examples*, *JHEP* **02** (2023) 021 [[2210.02907](#)].
- [6] C. Creque-Sarbinowski, S. Alexander, M. Kamionkowski and O. Philcox, *Parity-violating trispectrum from Chern-Simons gravity*, *JCAP* **11** (2023) 029 [[2303.04815](#)].
- [7] S. Jazayeri, S. Renaux-Petel, X. Tong, D. Werth and Y. Zhu, *Parity violation from emergent nonlocality during inflation*, *Phys. Rev. D* **108** (2023) 123523 [[2308.11315](#)].
- [8] T. Fujita, T. Murata, I. Obata and M. Shiraiishi, *Parity-violating scalar trispectrum from a rolling axion during inflation*, [2310.03551](#).
- [9] E. Vanzan, M. Kamionkowski and S.C. Hotinli, *Phenomenology of a vector-field-induced (and possibly parity breaking) compensated isocurvature perturbation*, [2311.18121](#).
- [10] T. Callister, L. Jenks, D. Holz and N. Yunes, *A New Probe of Gravitational Parity Violation Through (Non-)Observation of the Stochastic Gravitational-Wave Background*, [2312.12532](#).
- [11] G. Cabass, M.M. Ivanov and O.H.E. Philcox, *Colliders and ghosts: Constraining inflation with the parity-odd galaxy four-point function*, *Phys. Rev. D* **107** (2023) 023523 [[2210.16320](#)].
- [12] O.H.E. Philcox and J. Ereza, *Could Sample Variance be Responsible for the Parity-Violating Signal Seen in the BOSS Galaxy Survey?*, [2401.09523](#).
- [13] Y. Minami and E. Komatsu, *New Extraction of the Cosmic Birefringence from the Planck 2018 Polarization Data*, *Phys. Rev. Lett.* **125** (2020) 221301 [[2011.11254](#)].
- [14] P. Diego-Palazuelos et al., *Cosmic Birefringence from the Planck Data Release 4*, *Phys. Rev. Lett.* **128** (2022) 091302 [[2201.07682](#)].
- [15] J.R. Eskilt and E. Komatsu, *Improved constraints on cosmic birefringence from the WMAP and Planck cosmic microwave background polarization data*, *Phys. Rev. D* **106** (2022) 063503 [[2205.13962](#)].
- [16] O.H.E. Philcox, *Do the CMB Temperature Fluctuations Conserve Parity?*, *Phys. Rev. Lett.* **131** (2023) 181001 [[2303.12106](#)].
- [17] DESI COLLABORATION collaboration, *DESI 2024 VI: Cosmological Constraints from the Measurements of Baryon Acoustic Oscillations*, [2404.03002](#).
- [18] X. Xu, N. Padmanabhan, D.J. Eisenstein, K.T. Mehta and A.J. Cuesta, *A 2 per cent distance to $z = 0.35$ by reconstructing baryon acoustic oscillations - II. Fitting techniques*, *MNRAS* **427** (2012) 2146 [[1202.0091](#)].
- [19] Z. Slepian and D.J. Eisenstein, *Computing the three-point correlation function of galaxies in $\mathcal{O}(N^2)$ time*, *Mon. Not. Roy. Astron. Soc.* **454** (2015) 4142 [[1506.02040](#)].
- [20] F.-S. Kitaura et al., *The clustering of galaxies in the SDSS-III Baryon Oscillation Spectroscopic Survey: mock galaxy catalogues for the BOSS Final Data Release*, *Mon. Not. Roy. Astron. Soc.* **456** (2016) 4156 [[1509.06400](#)].

- [21] S.A. Rodríguez-Torres et al., *The clustering of galaxies in the SDSS-III Baryon Oscillation Spectroscopic Survey: modelling the clustering and halo occupation distribution of BOSS CMASS galaxies in the Final Data Release*, *Mon. Not. Roy. Astron. Soc.* **460** (2016) 1173 [1509.06404].
- [22] F. Villaescusa-Navarro, C. Hahn, E. Massara, A. Banerjee, A.M. Delgado, D.K. Ramanah et al., *The Quijote Simulations*, *ApJS* **250** (2020) 2 [1909.05273].
- [23] Z. Slepian et al., *Detection of baryon acoustic oscillation features in the large-scale three-point correlation function of SDSS BOSS DR12 CMASS galaxies*, *Mon. Not. Roy. Astron. Soc.* **469** (2017) 1738 [1607.06097].
- [24] S. Alam, M. Ata, S. Bailey, F. Beutler, D. Bizyaev, J.A. Blazek et al., *The clustering of galaxies in the completed SDSS-III Baryon Oscillation Spectroscopic Survey: cosmological analysis of the DR12 galaxy sample*, *MNRAS* **470** (2017) 2617 [1607.03155].
- [25] D.J. Eisenstein, D.H. Weinberg, E. Agol, H. Aihara, C. Allende Prieto, S.F. Anderson et al., *SDSS-III: Massive Spectroscopic Surveys of the Distant Universe, the Milky Way, and Extra-Solar Planetary Systems*, *AJ* **142** (2011) 72 [1101.1529].
- [26] K.S. Dawson, D.J. Schlegel, C.P. Ahn, S.F. Anderson, É. Aubourg, S. Bailey et al., *The Baryon Oscillation Spectroscopic Survey of SDSS-III*, *AJ* **145** (2013) 10 [1208.0022].
- [27] F. Beutler, H.-J. Seo, S. Saito, C.-H. Chuang, A.J. Cuesta, D.J. Eisenstein et al., *The clustering of galaxies in the completed SDSS-III Baryon Oscillation Spectroscopic Survey: anisotropic galaxy clustering in Fourier space*, *MNRAS* **466** (2017) 2242 [1607.03150].
- [28] F.S. Kitaura, G. Yepes and F. Prada, *Modelling baryon acoustic oscillations with perturbation theory and stochastic halo biasing.*, *MNRAS* **439** (2014) L21 [1307.3285].
- [29] B. Reid et al., *SDSS-III Baryon Oscillation Spectroscopic Survey Data Release 12: galaxy target selection and large scale structure catalogues*, *Mon. Not. Roy. Astron. Soc.* **455** (2016) 1553 [arXiv:1509.06529].
- [30] H.A. Feldman, N. Kaiser and J.A. Peacock, *Power-Spectrum Analysis of Three-dimensional Redshift Surveys*, *ApJ* **426** (1994) 23 [astro-ph/9304022].
- [31] H. Guo, I. Zehavi and Z. Zheng, *A New Method to Correct for Fiber Collisions in Galaxy Two-point Statistics*, *ApJ* **756** (2012) 127 [1111.6598].
- [32] A.J. Ross, F. Beutler, C.-H. Chuang, M. Pellejero-Ibanez, H.-J. Seo, M. Vargas-Magaña et al., *The clustering of galaxies in the completed SDSS-III Baryon Oscillation Spectroscopic Survey: observational systematics and baryon acoustic oscillations in the correlation function*, *MNRAS* **464** (2017) 1168 [1607.03145].
- [33] O.H.E. Philcox, J. Hou and Z. Slepian, *A First Detection of the Connected 4-Point Correlation Function of Galaxies Using the BOSS CMASS Sample*, *arXiv e-prints* (2021) arXiv:2108.01670 [2108.01670].
- [34] R.N. Cahn and Z. Slepian, *Isotropic N-point basis functions and their properties*, *J. Phys. A* **56** (2023) 325204 [2010.14418].
- [35] O.H.E. Philcox, Z. Slepian, J. Hou, C. Warner, R.N. Cahn and D.J. Eisenstein, *encore: an $O(N_g^2)$ estimator for galaxy N-point correlation functions*, *Mon. Not. Roy. Astron. Soc.* **509** (2021) 2457 [2105.08722].
- [36] S.D. Landy and A.S. Szalay, *Bias and Variance of Angular Correlation Functions*, *ApJ* **412** (1993) 64.
- [37] I. Szapudi and A.S. Szalay, *A New Class of Estimators for the N-Point Correlations*, *ApJ* **494** (1998) L41.

- [38] A. Chudaykin, M.M. Ivanov, O.H.E. Philcox and M. Simonović, *Nonlinear perturbation theory extension of the Boltzmann code CLASS*, *Phys. Rev. D* **102** (2020) 063533 [2004.10607].
- [39] P. Adari and A. Slosar, *Searching for Parity Violation in SDSS DR16 Lyman- α Forest Data*, 2405.04660.

A Deriving the analytic covariance

Recall from section 3.2 that the “analytic” covariance matrix $(C_{\text{ana}})_{ab} = \text{Cov}(\hat{\mathcal{E}}_a, \hat{\mathcal{E}}_b)$ is the estimator covariance under the approximations that $\delta_g(\mathbf{x})$ is a Gaussian field, and the survey geometry is a 3D periodic box with fiducial box volume V_{fid} . In this appendix, we will derive a closed-form expression for the analytic covariance. This was first derived in [4], building on 3PCF results from [19].

Our final expression for C_{ana} agrees with [4], but we have included a detailed derivation in this appendix for a few reasons. First, to make the paper self-contained. Second, because we do the calculation in a different way from [1], and an alternate approach may be pedagogically useful. Third, in order to comment on some details of the numerical implementation.

We checked that the output of our C_{ana} code agrees with with the output of the `npcf_cov` code from [1, 4], and with the public covariance matrix from [2]. This is an independent cross-check on results from [1, 2, 4], and also shows that the analysis in our paper is consistent with these previous studies.

A.1 Special function identities

Throughout this appendix, $C_{m_1 m_2 m_3}^{l_1 l_2 l_3}$ is compressed notation for the Wigner 3j symbol:

$$C_{m_1 m_2 m_3}^{l_1 l_2 l_3} \equiv \begin{pmatrix} l_1 & l_2 & l_3 \\ m_1 & m_2 & m_3 \end{pmatrix} \quad (\text{A.1})$$

We also define the quantity $G_{l_1 l_2 l_3}$ by:

$$G_{l_1 l_2 l_3} \equiv \sqrt{\frac{(2l_1 + 1)(2l_2 + 1)(2l_3 + 1)}{4\pi}} \begin{pmatrix} l_1 & l_2 & l_3 \\ 0 & 0 & 0 \end{pmatrix} \quad (\text{A.2})$$

Using this notation, the integral of three spherical harmonics is given by:

$$\int d^2\hat{\mathbf{r}} Y_{l_1 m_1}(\hat{\mathbf{r}}) Y_{l_2 m_2}(\hat{\mathbf{r}}) Y_{l_3 m_3}(\hat{\mathbf{r}}) = G_{l_1 l_2 l_3} C_{m_1 m_2 m_3}^{l_1 l_2 l_3} \quad (\text{A.3})$$

An equivalent identity expands the product of two spherical harmonics as a sum of spherical harmonics:

$$Y_{lm}(\hat{\mathbf{r}}) Y_{l'm'}(\hat{\mathbf{r}}) = \sum_{LM} G_{ll'L} C_{mm'M}^{ll'L} Y_{LM}^*(\hat{\mathbf{r}}) \quad (\text{A.4})$$

In appendix A.4, we will need the following angular integral involving four spherical harmonics:

$$\begin{aligned} & \int d^2\hat{\mathbf{r}} Y_{l_1 m_1}^*(\hat{\mathbf{r}}) Y_{l'_1 m'_1}^*(\hat{\mathbf{r}}) Y_{L_2 M_2}(\hat{\mathbf{r}}) Y_{L_3 M_3}(\hat{\mathbf{r}}) \\ &= \int d^2\hat{\mathbf{r}} \left(\sum_{L_1 M_1} G_{l_1 l'_1 L_1} C_{m_1 m'_1 M_1}^{l_1 l'_1 L_1} Y_{L_1 M_1}(\hat{\mathbf{r}}) \right) Y_{L_2 M_2}(\hat{\mathbf{r}}) Y_{L_3 M_3}(\hat{\mathbf{r}}) \\ &= \sum_{L_1 M_1} G_{l_1 l'_1 L_1} G_{L_1 L_2 L_3} C_{m_1 m'_1 M_1}^{l_1 l'_1 L_1} C_{M_1 M_2 M_3}^{L_1 L_2 L_3} \end{aligned} \quad (\text{A.5})$$

where we have used eq. (A.4) in the first line, and eq. (A.3) in the second line.

The following identity is one way of defining the Wigner 9j symbol:

$$\left\{ \begin{matrix} l_{11} & l_{12} & l_{13} \\ l_{21} & l_{22} & l_{23} \\ l_{31} & l_{32} & l_{33} \end{matrix} \right\} = \sum_{m_{ij}} \begin{pmatrix} l_{11} & l_{12} & l_{13} \\ m_{11} & m_{12} & m_{13} \end{pmatrix} \begin{pmatrix} l_{21} & l_{22} & l_{23} \\ m_{21} & m_{22} & m_{23} \end{pmatrix} \begin{pmatrix} l_{31} & l_{32} & l_{33} \\ m_{31} & m_{32} & m_{33} \end{pmatrix} \\ \times \begin{pmatrix} l_{11} & l_{21} & l_{31} \\ m_{11} & m_{21} & m_{31} \end{pmatrix} \begin{pmatrix} l_{12} & l_{22} & l_{32} \\ m_{12} & m_{22} & m_{32} \end{pmatrix} \begin{pmatrix} l_{13} & l_{23} & l_{33} \\ m_{13} & m_{23} & m_{33} \end{pmatrix} \quad (\text{A.6})$$

A.2 Strategy of the calculation

Restricting to the parity-odd case ($\sum l_i$ odd), we rewrite the estimator (3.3) as:

$$\widehat{\mathcal{E}}_{l_1 l_2 l_3}^{\beta_1 \beta_2 \beta_3} = -\frac{1}{V_{\text{fid}}} \sum_{m_i} C_{m_1 m_2 m_3}^{l_1 l_2 l_3} \int d^3 \mathbf{x} \delta_{\mathbf{g}}(\mathbf{x}) \prod_{i=1}^3 \delta_{l_i m_i}^{\beta_i}(\mathbf{x}) \quad (\text{A.7})$$

where we have defined the field:

$$\delta_{lm}^{\beta}(\mathbf{x}) \equiv \int d^3 \mathbf{r} W_{lm}^{\beta}(\mathbf{r}) \delta_{\mathbf{g}}(\mathbf{x} + \mathbf{r}) \quad (\text{A.8})$$

We write the covariance as (defining $\int_{\mathbf{xx}'} = \int d^3 \mathbf{x} d^3 \mathbf{x}'$):

$$\text{Cov}(\widehat{\mathcal{E}}_{l_1 l_2 l_3}^{\beta_1 \beta_2 \beta_3}, \widehat{\mathcal{E}}_{l'_1 l'_2 l'_3}^{\beta'_1 \beta'_2 \beta'_3 *}) = -\frac{1}{V_{\text{fid}}^2} \sum_{m_i m'_j} C_{m_1 m_2 m_3}^{l_1 l_2 l_3} C_{m'_1 m'_2 m'_3}^{l'_1 l'_2 l'_3} \\ \times \int_{\mathbf{xx}'} \left\langle \left(\delta_{\mathbf{g}}(\mathbf{x}) \prod_{i=1}^3 \delta_{l_i m_i}^{\beta_i}(\mathbf{x}) \right) \left(\delta_{\mathbf{g}}(\mathbf{x}') \prod_{j=1}^3 \delta_{l'_j m'_j}^{\beta'_j}(\mathbf{x}') \right) \right\rangle \quad (\text{A.9})$$

In this expression, the expectation value $\langle \dots \rangle$ is an eight-point function in the field $\delta_{\mathbf{g}}$. Since we are assuming $\delta_{\mathbf{g}}$ is a Gaussian field, we can use Wick's theorem to write the eight-point function as a sum of 24 contractions. We define T and U to be the following contractions:

$$T_{l_1 l_2 l_3 l'_1 l'_2 l'_3}^{\beta_1 \beta_2 \beta_3 \beta'_1 \beta'_2 \beta'_3} = -\frac{1}{V_{\text{fid}}^2} \sum_{m_i m'_j} C_{m_1 m_2 m_3}^{l_1 l_2 l_3} C_{m'_1 m'_2 m'_3}^{l'_1 l'_2 l'_3} \\ \times \int_{\mathbf{xx}'} \left(\delta_{\mathbf{g}}(\mathbf{x}) \delta_{l_1 m_1}^{\beta_1}(\mathbf{x}) \delta_{l_2 m_2}^{\beta_2}(\mathbf{x}) \delta_{l_3 m_3}^{\beta_3}(\mathbf{x}) \right) \left(\delta_{\mathbf{g}}(\mathbf{x}') \delta_{l'_1 m'_1}^{\beta'_1}(\mathbf{x}') \delta_{l'_2 m'_2}^{\beta'_2}(\mathbf{x}') \delta_{l'_3 m'_3}^{\beta'_3}(\mathbf{x}') \right) \quad (\text{A.10})$$

$$U_{l_1 l_2 l_3 l'_1 l'_2 l'_3}^{\beta_1 \beta_2 \beta_3 \beta'_1 \beta'_2 \beta'_3} = -\frac{1}{V_{\text{fid}}^2} \sum_{m_i m'_j} C_{m_1 m_2 m_3}^{l_1 l_2 l_3} C_{m'_1 m'_2 m'_3}^{l'_1 l'_2 l'_3} \\ \times \int_{\mathbf{xx}'} \left(\delta_{\mathbf{g}}(\mathbf{x}) \delta_{l_1 m_1}^{\beta_1}(\mathbf{x}) \delta_{l_2 m_2}^{\beta_2}(\mathbf{x}) \delta_{l_3 m_3}^{\beta_3}(\mathbf{x}) \right) \left(\delta_{\mathbf{g}}(\mathbf{x}') \delta_{l'_1 m'_1}^{\beta'_1}(\mathbf{x}') \delta_{l'_2 m'_2}^{\beta'_2}(\mathbf{x}') \delta_{l'_3 m'_3}^{\beta'_3}(\mathbf{x}') \right) \quad (\text{A.11})$$

Additionally, there are 5 terms obtained by permuting indices in T , and 17 terms obtained by permuting indices in U . These terms have some nontrivial signs. To see this, consider the

contraction \bar{T} obtained from T by exchanging the roles of $\delta_{l_1 m_1}^{\beta_1}(\mathbf{x})$ and $\delta_{l_2 m_2}^{\beta_2}(\mathbf{x})$:

$$\begin{aligned} \bar{T}_{l_1 l_2 l_3 l'_1 l'_2 l'_3}^{\beta_1 \beta_2 \beta_3 \beta'_1 \beta'_2 \beta'_3} &= -\frac{1}{V_{\text{fid}}^2} \sum_{m_i m'_j} C_{m_1 m_2 m_3}^{l_1 l_2 l_3} C_{m'_1 m'_2 m'_3}^{l'_1 l'_2 l'_3} \\ &\times \int_{\mathbf{x}\mathbf{x}'} \left(\delta_{\mathbf{g}}(\mathbf{x}) \delta_{l_1 m_1}^{\beta_1}(\mathbf{x}) \delta_{l_2 m_2}^{\beta_2}(\mathbf{x}) \delta_{l_3 m_3}^{\beta_3}(\mathbf{x}) \right) \left(\delta_{\mathbf{g}}(\mathbf{x}') \delta_{l'_1 m'_1}^{\beta'_1}(\mathbf{x}') \delta_{l'_2 m'_2}^{\beta'_2}(\mathbf{x}') \delta_{l'_3 m'_3}^{\beta'_3}(\mathbf{x}') \right) \end{aligned} \quad (\text{A.12})$$

Comparing to the definition (A.10) of T , the two contractions are related by the index permutation $(l_1, \beta_1) \leftrightarrow (l_2, \beta_2)$, but we also get an extra minus sign, since $C_{m_2 m_1 m_3}^{l_2 l_1 l_3} = (-1)^{\sum l_i} C_{m_1 m_2 m_3}^{l_1 l_2 l_3}$, and $\sum l_i$ is odd. Therefore:

$$\bar{T}_{l_1 l_2 l_3 l'_1 l'_2 l'_3}^{\beta_1 \beta_2 \beta_3 \beta'_1 \beta'_2 \beta'_3} = -T_{l_2 l_1 l_3 l'_1 l'_2 l'_3}^{\beta_2 \beta_1 \beta_3 \beta'_1 \beta'_2 \beta'_3} \quad (\text{A.13})$$

Applying similar logic to all 24 contractions, the total covariance can be written as:

$$\begin{aligned} \text{Cov}(\widehat{\mathcal{E}}_{l_1 l_2 l_3}^{\beta_1 \beta_2 \beta_3}, \widehat{\mathcal{E}}_{l'_1 l'_2 l'_3}^{\beta'_1 \beta'_2 \beta'_3*}) &= \left(T_{l_1 l_2 l_3 l'_1 l'_2 l'_3}^{\beta_1 \beta_2 \beta_3 \beta'_1 \beta'_2 \beta'_3} + U_{l_1 l_2 l_3 l'_1 l'_2 l'_3}^{\beta_1 \beta_2 \beta_3 \beta'_1 \beta'_2 \beta'_3} + U_{l_1 l_2 l_3 l'_2 l'_3 l'_1}^{\beta_1 \beta_2 \beta_3 \beta'_2 \beta'_3 \beta'_1} + U_{l_1 l_2 l_3 l'_3 l'_1 l'_2}^{\beta_1 \beta_2 \beta_3 \beta'_3 \beta'_1 \beta'_2} \right) \\ &\quad + \left(2 \text{ even permutations of } (\beta_1, l_1), (\beta_2, l_2), (\beta_3, l_3) \right) \\ &\quad - \left(3 \text{ odd permutations of } (\beta_1, l_1), (\beta_2, l_2), (\beta_3, l_3) \right) \end{aligned} \quad (\text{A.14})$$

It remains to compute T, U . In appendix A.3, we will compute the following two-point functions, which are needed to evaluate contractions:

$$\langle \delta_{\mathbf{g}}(\mathbf{x}) \delta_{\mathbf{g}}(\mathbf{x}') \rangle \quad \langle \delta_{\mathbf{g}}(\mathbf{x}) \delta_{l' m'}^{\beta'}(\mathbf{x}') \rangle \quad \langle \delta_{l m}^{\beta}(\mathbf{x}) \delta_{l' m'}^{\beta'}(\mathbf{x}') \rangle \quad (\text{A.15})$$

Then we will compute T, U in appendix A.4.

A.3 Computing the two-point functions in eq. (A.15)

The first two-point function in eq. (A.15) is the usual galaxy correlation function $\xi(r) = \langle \delta_{\mathbf{g}}(\mathbf{x}) \delta_{\mathbf{g}}(\mathbf{x} + \mathbf{r}) \rangle$. This is straightforward to compute in Fourier space:

$$\begin{aligned} \xi(r) &= \int \frac{d^3 \mathbf{k}}{(2\pi)^3} P_{\mathbf{g}}(k) e^{i\mathbf{k} \cdot \mathbf{r}} \\ &= \int_0^\infty dk \frac{k^2}{2\pi^2} P_{\mathbf{g}}(k) j_0(kr) \end{aligned} \quad (\text{A.16})$$

The remaining two-point functions in eq. (A.15) can be calculated similarly, but the details are a bit more complicated, since the angular integrals contains spherical harmonics and are nontrivial. First, we note that $\delta_{l m}^{\beta}$ can be written as a convolution. Starting from the

definition (A.8):

$$\begin{aligned}
\delta_{lm}^\beta(\mathbf{x}) &= \int d^3\mathbf{r} W_{lm}^\beta(\mathbf{r}) \delta_g(\mathbf{x} + \mathbf{r}) \\
&= (-1)^l \int d^3\mathbf{r} W_{lm}^\beta(-\mathbf{r}) \delta_g(\mathbf{x} + \mathbf{r}) \quad \text{since } W_{lm}^\beta(\mathbf{r}) = (-1)^l W_{lm}^\beta(-\mathbf{r}) \\
&= (-1)^l \underbrace{W_{lm}^\beta \star \delta_g}_{\text{convolution}} \tag{A.17}
\end{aligned}$$

Therefore, $\delta_{lm}^\beta(\mathbf{k})$ is given in Fourier space by multiplication:

$$\delta_{lm}^\beta(\mathbf{k}) = (-1)^l \widetilde{W}_{lm}^\beta(\mathbf{k}) \delta_g(\mathbf{k}) \tag{A.18}$$

where $\widetilde{W}_{lm}^\beta(\mathbf{k})$ is the Fourier transform of the function $W_{lm}^\beta(\mathbf{r})$ defined in eq. (3.2) above. We compute $\widetilde{W}_{lm}^\beta(\mathbf{k})$ as follows:

$$\begin{aligned}
\widetilde{W}_{lm}^\beta(\mathbf{k}) &= \int d^3\mathbf{r} W_{lm}^\beta(\mathbf{r}) e^{-i\mathbf{k}\cdot\mathbf{r}} \\
&= \frac{4\pi}{V_\beta} \int_{r \in \beta} d^3\mathbf{r} Y_{lm}^*(\hat{\mathbf{r}}) \left[\sum_{LM} 4\pi (-i)^L j_L(kr) Y_{LM}(\hat{\mathbf{r}}) Y_{LM}^*(\hat{\mathbf{k}}) \right] \\
&= \frac{4\pi}{V_\beta} \int_{r \in \beta} dr 4\pi r^2 (-i)^l j_l(kr) Y_{lm}^*(\hat{\mathbf{k}}) \\
&= 4\pi (-i)^l B_l^\beta(k) Y_{lm}^*(\hat{\mathbf{k}}) \tag{A.19}
\end{aligned}$$

where we define the ‘‘binned’’ Bessel function $B_l^\beta(k)$ by bin-averaging $j_l(kr)$:

$$B_l^\beta(k) = \frac{\int_{r \in \beta} dr r^2 j_l(kr)}{\int_{r \in \beta} dr r^2} \tag{A.20}$$

See appendix A.5 for comments on numerical evaluation of $B_l^\beta(k)$.

Returning to the two-point functions in eq. (A.15), we can now compute $\langle \delta_g(\mathbf{x}) \delta_{l'm'}^{\beta'}(\mathbf{x} + \mathbf{r}) \rangle$ as follows:

$$\begin{aligned}
\langle \delta_g(\mathbf{x}) \delta_{l'm'}^{\beta'}(\mathbf{x} + \mathbf{r}) \rangle &= \left\langle \left(\int \frac{d^3\mathbf{k}}{(2\pi)^3} \delta_g(\mathbf{k}) e^{i\mathbf{k}\cdot\mathbf{x}} \right) \left((-1)^{l'} \int \frac{d^3\mathbf{k}'}{(2\pi)^3} \widetilde{W}_{l'm'}^{\beta'}(\mathbf{k}') \delta_g(\mathbf{k}') e^{i\mathbf{k}'\cdot(\mathbf{x}+\mathbf{r})} \right) \right\rangle \\
&= (-1)^{l'} \int \frac{d^3\mathbf{k}}{(2\pi)^3} P_g(k) \widetilde{W}_{l'm'}^{\beta'}(-\mathbf{k}) e^{-i\mathbf{k}\cdot\mathbf{r}} \\
&= (-1)^{l'} \int \frac{d^3\mathbf{k}}{(2\pi)^3} P_g(k) \left(4\pi (+i)^{l'} B_{l'}^{\beta'}(k) Y_{l'm'}^*(\hat{\mathbf{k}}) \right) \\
&\quad \times \left(\sum_{LM} 4\pi (-i)^L j_L(kr) Y_{LM}(\hat{\mathbf{k}}) Y_{LM}^*(\hat{\mathbf{r}}) \right) \\
&= 4\pi (-1)^{l'} H_{l'}^{\beta'}(k) Y_{l'm'}^*(\hat{\mathbf{r}}) \tag{A.21}
\end{aligned}$$

where the radial function $H_l^\beta(r)$ is defined by:

$$H_l^\beta(r) \equiv \int_0^\infty dk \frac{k^2}{2\pi^2} P_g(k) B_l^\beta(k) j_l(kr) \quad (\text{A.22})$$

Similarly, we can compute the third two-point function in eq. (A.15):

$$\begin{aligned} \langle \delta_{lm}^\beta(\mathbf{x}) \delta_{l'm'}^{\beta'}(\mathbf{x} + \mathbf{r}) \rangle &= (-1)^{l+l'} \int \frac{d^3\mathbf{k}}{(2\pi)^3} P_g(k) \widetilde{W}_{lm}^\beta(\mathbf{k}) \widetilde{W}_{l'm'}^{\beta'}(-\mathbf{k}) e^{-i\mathbf{k}\cdot\mathbf{r}} \\ &= (-1)^{l+l'} \int \frac{d^3\mathbf{k}}{(2\pi)^3} P_g(k) \left(4\pi(-i)^l B_l^\beta(k) Y_{lm}^*(\hat{\mathbf{k}}) \right) \\ &\quad \times \left(4\pi(+i)^{l'} B_{l'}^{\beta'}(k) Y_{l'm'}^*(\hat{\mathbf{k}}) \right) \\ &\quad \times \left(\sum_{LM} 4\pi(-i)^L j_L(kr) Y_{LM}^*(\hat{\mathbf{k}}) Y_{LM}(\hat{\mathbf{r}}) \right) \\ &= (4\pi)^2 \sum_{LM} i^{l-l'-L} \left(\int \frac{k^2 dk}{2\pi^2} P_g(k) B_l^\beta(k) B_{l'}^{\beta'}(k) j_L(kr) \right) \\ &\quad \times \left(\int d^2\hat{\mathbf{k}} Y_{lm}^*(\hat{\mathbf{k}}) Y_{l'm'}^*(\hat{\mathbf{k}}) Y_{LM}(\hat{\mathbf{k}}) \right) Y_{LM}(\hat{\mathbf{r}}) \\ &= (4\pi)^2 \sum_{LM} i^{l-l'-L} F_{l'l}^{\beta\beta'}(r) G_{l'l} C_{mm'M}^{l'l} Y_{LM}(\hat{\mathbf{r}}) \end{aligned} \quad (\text{A.23})$$

where the radial function $F_{l'l}^{\beta\beta'}(r)$ is defined by:

$$F_{l'l}^{\beta\beta'}(r) \equiv \int_0^\infty dk \frac{k^2}{2\pi^2} P_g(k) B_l^\beta(k) B_{l'}^{\beta'}(k) j_L(kr) \quad (\text{A.24})$$

A.4 Computing $T_{l_1 l_2 l_3 l'_1 l'_2 l'_3}^{\beta_1 \beta_2 \beta_3 \beta'_1 \beta'_2 \beta'_3}$ and $U_{l_1 l_2 l_3 l'_1 l'_2 l'_3}^{\beta_1 \beta_2 \beta_3 \beta'_1 \beta'_2 \beta'_3}$

Starting from the definition (A.10) of T , we write the Wick contractions as two-point functions:

$$T_{l_1 l_2 l_3 l'_1 l'_2 l'_3}^{\beta_1 \beta_2 \beta_3 \beta'_1 \beta'_2 \beta'_3} = -\frac{1}{V_{\text{fid}}^2} \sum_{m_i m'_j} C_{m_1 m_2 m_3}^{l_1 l_2 l_3} C_{m'_1 m'_2 m'_3}^{l'_1 l'_2 l'_3} \int_{\mathbf{xx}'} \langle \delta_g(\mathbf{x}) \delta_g(\mathbf{x}') \rangle \prod_{k=1}^3 \langle \delta_{l_k m_k}^{\beta_k}(\mathbf{x}) \delta_{l'_k m'_k}^{\beta'_k}(\mathbf{x}') \rangle \quad (\text{A.25})$$

Plugging in the two-point functions in eqs. (A.16) and (A.23), we get:

$$\begin{aligned} T_{l_1 l_2 l_3 l'_1 l'_2 l'_3}^{\beta_1 \beta_2 \beta_3 \beta'_1 \beta'_2 \beta'_3} &= -\frac{(4\pi)^6}{V_{\text{fid}}} \sum_{m_i m'_j} C_{m_1 m_2 m_3}^{l_1 l_2 l_3} C_{m'_1 m'_2 m'_3}^{l'_1 l'_2 l'_3} \\ &\quad \times \int d^3\mathbf{r} \xi(r) \prod_{k=1}^3 \left(\sum_{L_k M_k} i^{l_k - l'_k - L_k} F_{l'_k l_k}^{\beta_k \beta'_k}(r) G_{l'_k l_k} C_{m_k m'_k M_k}^{l_k l'_k L_k} Y_{L_k M_k}(\hat{\mathbf{r}}) \right) \end{aligned} \quad (\text{A.26})$$

We simplify the following subexpression, obtained by bringing the angular integral ($\int d^2\hat{\mathbf{r}}$) and all 9 m -sums to the inside:

$$\begin{aligned}
& \sum_{m_i m'_j} C_{m_1 m_2 m_3}^{l_1 l_2 l_3} C_{m'_1 m'_2 m'_3}^{l'_1 l'_2 l'_3} \int d^2\hat{\mathbf{r}} \prod_{k=1}^3 \left(\sum_{M_k} C_{m_k m'_k M_k}^{l_k l'_k L_k} Y_{L_k M_k}(\hat{\mathbf{r}}) \right) \\
&= G_{L_1 L_2 L_3} \sum_{m_i m'_j M_k} C_{m_1 m_2 m_3}^{l_1 l_2 l_3} C_{m'_1 m'_2 m'_3}^{l'_1 l'_2 l'_3} C_{m_1 m'_1 M_1}^{l_1 l'_1 L_1} C_{m_2 m'_2 M_2}^{l_2 l'_2 L_2} C_{m_3 m'_3 M_3}^{l_3 l'_3 L_3} C_{M_1 M_2 M_3}^{L_1 L_2 L_3} \\
&= G_{L_1 L_2 L_3} \left\{ \begin{array}{ccc} l_1 & l_2 & l_3 \\ l'_1 & l'_2 & l'_3 \\ L_1 & L_2 & L_3 \end{array} \right\} \tag{A.27}
\end{aligned}$$

In the first line we used eq. (A.3), and in the second line we used definition (A.6) of the 9j symbol. Plugging eq. (A.27) into eq. (A.26), we get our final expression for T :

$$\begin{aligned}
T_{l_1 l_2 l_3 l'_1 l'_2 l'_3}^{\beta_1 \beta_2 \beta_3 \beta'_1 \beta'_2 \beta'_3} &= \frac{(4\pi)^6}{V_{\text{fid}}} \sum_{L_1 L_2 L_3} (-i)^{\sum_k (l_k + l'_k + L_k)} G_{l_1 l'_1 L_1} G_{l_2 l'_2 L_2} G_{l_3 l'_3 L_3} G_{L_1 L_2 L_3} \left\{ \begin{array}{ccc} l_1 & l_2 & l_3 \\ l'_1 & l'_2 & l'_3 \\ L_1 & L_2 & L_3 \end{array} \right\} \\
&\times \int_0^\infty dr r^2 \xi(r) F_{l_1 l'_1 L_1}^{\beta_1 \beta'_1}(r) F_{l_2 l'_2 L_2}^{\beta_2 \beta'_2}(r) F_{l_3 l'_3 L_3}^{\beta_3 \beta'_3}(r) \tag{A.28}
\end{aligned}$$

Similarly, starting from the definition (A.11) of U , we write the Wick contractions as two-point functions:

$$\begin{aligned}
U_{l_1 l_2 l_3 l'_1 l'_2 l'_3}^{\beta_1 \beta_2 \beta_3 \beta'_1 \beta'_2 \beta'_3} &= -\frac{1}{V_{\text{fid}}^2} \sum_{m_i m'_j} C_{m_1 m_2 m_3}^{l_1 l_2 l_3} C_{m'_1 m'_2 m'_3}^{l'_1 l'_2 l'_3} \\
&\times \int_{\mathbf{x}\mathbf{x}'} \langle \delta_{\mathbf{g}}(\mathbf{x}) \delta_{l'_1 m'_1}^{\beta'_1}(\mathbf{x}') \rangle \langle \delta_{l_1 m_1}^{\beta_1}(\mathbf{x}) \delta_{\mathbf{g}}(\mathbf{x}') \rangle \prod_{k=2}^3 \langle \delta_{l_k m_k}^{\beta_k}(\mathbf{x}) \delta_{l'_k m'_k}^{\beta'_k}(\mathbf{x}') \rangle \tag{A.29}
\end{aligned}$$

Plugging in the two-point functions in eqs. (A.21) and (A.23), this becomes:

$$\begin{aligned}
U_{l_1 l_2 l_3 l'_1 l'_2 l'_3}^{\beta_1 \beta_2 \beta_3 \beta'_1 \beta'_2 \beta'_3} &= -\frac{(4\pi)^6}{V_{\text{fid}}} \sum_{m_i m'_j} C_{m_1 m_2 m_3}^{l_1 l_2 l_3} C_{m'_1 m'_2 m'_3}^{l'_1 l'_2 l'_3} \\
&\times \int d^3\mathbf{r} \left((-1)^{l'_1} H_{l'_1}^{\beta'_1}(r) Y_{l'_1 m'_1}^*(\hat{\mathbf{r}}) \right) \left(H_{l_1}^{\beta_1}(r) Y_{l_1 m_1}^*(\hat{\mathbf{r}}) \right) \\
&\times \prod_{k=2}^3 \left(\sum_{L_k M_k} i^{l_k - l'_k - L_k} F_{l_k l'_k L_k}^{\beta_k \beta'_k}(r) G_{l_k l'_k L_k} C_{m_k m'_k M_k}^{l_k l'_k L_k} Y_{L_k M_k}(\hat{\mathbf{r}}) \right) \tag{A.30}
\end{aligned}$$

We simplify the following subexpression, obtained by bringing the angular integral ($\int d^2\hat{\mathbf{r}}$)

and all eight m -sums to the inside:

$$\begin{aligned}
& \sum_{m_i m'_j} C_{m_1 m_2 m_3}^{l_1 l_2 l_3} C_{m'_1 m'_2 m'_3}^{l'_1 l'_2 l'_3} \int d^2 \hat{\mathbf{r}} Y_{l_1 m_1}^*(\hat{\mathbf{r}}) Y_{l'_1 m'_1}^*(\hat{\mathbf{r}}) \prod_{k=2}^3 \left(\sum_{M_k} C_{m_k m'_k M_k}^{l_k l'_k L_k} Y_{L_k M_k}(\hat{\mathbf{r}}) \right) \\
&= \sum_{m_i m'_j} \sum_{M_2 M_3} C_{m_1 m_2 m_3}^{l_1 l_2 l_3} C_{m'_1 m'_2 m'_3}^{l'_1 l'_2 l'_3} C_{m_2 m'_2 M_2}^{l_2 l'_2 L_2} C_{m_3 m'_3 M_3}^{l_3 l'_3 L_3} \\
&\quad \times \sum_{L_1 M_1} G_{l_1 l'_1 L_1} G_{L_1 L_2 L_3} C_{m_1 m'_1 M_1}^{l_1 l'_1 L_1} C_{M_1 M_2 M_3}^{L_1 L_2 L_3} \\
&= \sum_{L_1} G_{l_1 l'_1 L_1} G_{L_1 L_2 L_3} \left\{ \begin{array}{ccc} l_1 & l_2 & l_3 \\ l'_1 & l'_2 & l'_3 \\ L_1 & L_2 & L_3 \end{array} \right\} \tag{A.31}
\end{aligned}$$

In the first line, we used eq. (A.4), and in the second line we used the definition (A.6) of the 9j symbol. Plugging eq. (A.31) back into eq. (A.30), we get our final expression for U :

$$\begin{aligned}
U_{l_1 l_2 l_3 l'_1 l'_2 l'_3}^{\beta_1 \beta_2 \beta_3 \beta'_1 \beta'_2 \beta'_3} &= \frac{(4\pi)^6}{V_{\text{fid}}} \sum_{L_1 L_2 L_3} i^{l_2+l'_2-L_2} i^{l_3+l'_3-L_3} G_{l_1 l'_1 L_1} G_{l_2 l'_2 L_2} G_{l_3 l'_3 L_3} G_{L_1 L_2 L_3} \left\{ \begin{array}{ccc} l_1 & l_2 & l_3 \\ l'_1 & l'_2 & l'_3 \\ L_1 & L_2 & L_3 \end{array} \right\} \\
&\quad \times \int_0^\infty dr r^2 H_{l_1}^{\beta_1}(r) H_{l'_1}^{\beta'_1}(r) F_{l_2 l'_2 L_2}^{\beta_2 \beta'_2}(r) F_{l_3 l'_3 L_3}^{\beta_3 \beta'_3}(r) \tag{A.32}
\end{aligned}$$

A.5 Numerical evaluation of the binned Bessel function $B_l^\beta(k)$

In eq. (A.20), we defined the binned Bessel function $B_l^\beta(k)$. Numerical computation of $B_l^\beta(k)$ is nontrivial, and deserves some discussion. First, we write $B_l^\beta(k)$ as:

$$B_l^\beta(k) = 3 \frac{A_l(kR_{\text{max}}) - A_l(kR_{\text{min}})}{(kR_{\text{max}})^3 - (kR_{\text{min}})^3} \quad \text{where } \beta = [R_{\text{min}}, R_{\text{max}}] \tag{A.33}$$

where $A_l(x)$ is the antiderivative of $x^2 j_l(x)$:

$$A_l(x) \equiv \int_0^x dx' x'^2 j_l(x') \tag{A.34}$$

To compute $A_l(x)$, we use different approaches for small and large x . For $x \gtrsim 1$, we use the exact expressions:

$$\begin{aligned}
A_0(x) &= \sin(x) - x \cos(x) \\
A_1(x) &= 2(1 - \cos(x)) - x \sin(x) \\
A_2(x) &= x \cos(x) - 4 \sin(x) + 3 \text{Si}(x) \\
A_3(x) &= x \sin(x) + 7 \cos(x) - 15 \frac{\sin(x)}{x} + 8 \\
A_4(x) &= -x \cos(x) + 11 \sin(x) + \frac{105 \cos(x)}{2} \frac{1}{x} - \frac{105 \sin(x)}{2} \frac{1}{x^2} + \frac{15}{2} \text{Si}(x) \tag{A.35}
\end{aligned}$$

where the special function $\text{Si}(x) \equiv \int_0^x dt (\sin(t))/t$ can be computed using standard libraries.

For $x \lesssim 1$, the exact expressions in eq. (A.35) are numerically unstable, so to improve numerical accuracy, our code can switch to the series expansion for small arguments:

$$A_l(x) = \sum_{m=0}^{\infty} \frac{(-1)^m}{2^m m! (2m+2l+1)!!} \frac{x^{2m+l+3}}{2m+l+3} \quad (\text{A.36})$$

where $(2n+1)!! \equiv (2n+1)(2n-1)\dots(3)(1)$. However, we have found that this change does not meaningfully impact the final statistical significances when computing χ^2 , χ_{\times}^2 , and χ_{null}^2 .

A.6 Convergence tests for the analytic covariance matrix

As explained in section 3.2, the analytic covariance C_{ana} depends on integration parameters $(k_{\text{max}}, N_k, r_{\text{max}}, N_r)$. Our fiducial choices for these parameters are taken from [4]: $k_{\text{max}} = 5 h \text{ Mpc}^{-1}$, $N_k = 5000$, $r_{\text{max}} = 1000 h^{-1} \text{ Mpc}$, $N_r = 4100$. In this section, we will show that these fiducial parameters are chosen conservatively enough that this choice does not affect the rest of the analysis, i. e. the integrals producing C_{ana} are converged.

In order to compare covariance matrices C_{ana} with different choices of integration parameters, we define the following distance function $J(C_1, C_2)$ between *symmetric positive definite* matrices C_1, C_2 :

$$\begin{aligned} J(C_1, C_2) &= \text{Tr} \left(\frac{1}{4} C_1 C_2^{-1} + \frac{1}{4} C_2 C_1^{-1} - \frac{1}{2} I \right) \\ &= \frac{1}{4} \text{Tr} \left[\Delta^2 (1 + \Delta)^{-1} \right] \quad \text{where } \Delta \equiv C_2^{-1} (C_1 - C_2) \end{aligned} \quad (\text{A.37})$$

where the second line is more numerically stable as $C_1 \rightarrow C_2$. To motivate this choice of distance function, we state some key properties of J (with proofs omitted for brevity):

- $J(C_1, C_2) \geq 0$, with $J(C_1, C_2) = 0$ if and only if $C_1 = C_2$.
- Basis independence: if $C'_i = A C_i A^T$ where A is invertible, then $J(C'_1, C'_2) = J(C_1, C_2)$.
- Statistical interpretation: $J(C_1, C_2)$ is the symmetrized KL-divergence $(\text{KL}(\rho_1, \rho_2) + \text{KL}(\rho_2, \rho_1))/2$, where $\rho_i(x) \equiv \text{Det}(2\pi C_i)^{-1/2} \exp(-x^T C_i^{-1} x/2)$ is a multivariate Gaussian probability density function (PDF) with covariance C_i . Thus, $J(C_1, C_2)$ quantifies statistical distinguishability of the PDFs ρ_1, ρ_2 : they can be distinguished with N samples if and only if $J(C_1, C_2) \ll (1/N)$.

To test convergence of C_{ana} with respect to an integration parameter (say k_{max}), we compute C_{ana} twice using different parameter values (say fiducial $k_{\text{max}}^{\text{fid}} = 5 h \text{ Mpc}^{-1}$ and “high” $k_{\text{max}} = 10 h \text{ Mpc}^{-1}$), and verify that the two covariance matrices C, C' satisfy $J(C, C') \ll 1$. This test shows that changing the parameter from its fiducial value to a conservative value produces a nearly indistinguishable covariance matrix. This test effectively examines the entire covariance matrix, and is more powerful than testing a few specific matrix entries for convergence.

We apply this convergence test systematically, one integration parameter at a time:

$$\begin{aligned} J(C_{\text{ana}}^{\text{fid}}, C_{\text{ana}}^{\text{high } k_{\text{max}}}) &= 7.3058 \times 10^{-13} && \text{where high } k_{\text{max}} = 10 h \text{ Mpc}^{-1} \\ J(C_{\text{ana}}^{\text{fid}}, C_{\text{ana}}^{\text{high } N_k}) &= 2.7735 \times 10^{-13} && \text{where high } N_k = 10000 \\ J(C_{\text{ana}}^{\text{fid}}, C_{\text{ana}}^{\text{low } r_{\text{max}}}) &= 4.9609 \times 10^{-16} && \text{where low } r_{\text{max}} = 500 h \text{ Mpc} \\ J(C_{\text{ana}}^{\text{fid}}, C_{\text{ana}}^{\text{high } N_r}) &= 1.1658 \times 10^{-9} && \text{where high } N_r = 8200 \end{aligned} \quad (\text{A.38})$$

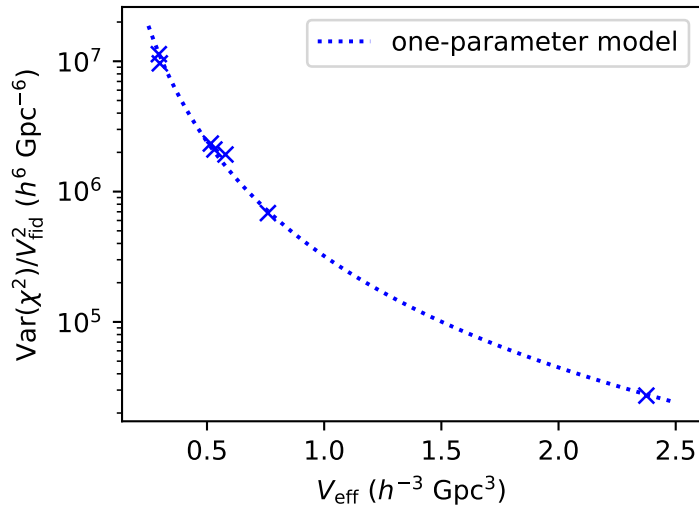


Figure 7. Each cross represents values of $(V_{\text{eff}}, \text{Var}(\chi^2))$ from one region in table 3. The dashed line is the one-parameter model in eq. (B.6).

Since all J -values are small, we conclude that our fiducial values of $(k_{\text{max}}, N_k, r_{\text{max}}, N_r)$ have been chosen conservatively enough to converge. Note that when we vary k_{max} , we leave the Gaussian smoothing scale (see eq. (3.7)) fixed at $k_0 = 1 h \text{ Mpc}^{-1}$.

B Why is $\text{Var}(\chi_{\times}^2)$ smaller than $\text{Var}(\chi^2)$?

Our new statistic χ_{\times}^2 is a more robust version of χ^2 . Empirically, we found that χ_{\times}^2 is also more statistically optimal than χ^2 , in the sense that $\text{Var}(\chi_{\times}^2) < \text{Var}(\chi^2)$. We initially found this counterintuitive, since χ_{\times}^2 uses less sky area than χ^2 (due to gaps between patches), and also throws away information from autocorrelating $\hat{\mathcal{E}}_a$ in the same patch. In this appendix, we will show that this is a non-Gaussian finite-volume effect, i. e. the inequality $\text{Var}(\chi_{\times}^2) < \text{Var}(\chi^2)$ would be reversed for a larger survey.

B.1 A one-parameter model for $\text{Var}(\chi^2)$

In this appendix, we use the term “region” to mean either the CMASS-NGC survey, the CMASSLOWZTOT-SGC survey, or a patch (in the sense of section 4.1) comprising one of these surveys. (A total of 7 regions can be defined in this way.)

For any such region, we can define the statistic $\chi^2 = \hat{\mathcal{E}}_a (C_{\text{ana}}^{-1})^{ab} \hat{\mathcal{E}}_b$. Recall from eq. (4.6) that we can also define the effective volume V_{eff} of the region by:

$$V_{\text{eff}} \equiv \frac{V_{\text{fid}} N_{\text{dof}}}{\text{Tr}(C_{\text{ana}}^{-1} C_{\text{mock}})} \quad (\text{B.1})$$

Values of V_{eff} for all 7 regions were given previously in table 3.

In figure 7 we plot V_{eff} and the variance $\text{Var}(\chi^2)$ for each region. The purpose of this section is to describe an analytic model (represented by the dotted curve in figure 7), with a single free parameter V_{thresh} , which does a good job of fitting all 7 points.

Let T_{abcd} be the *connected* four-point function of the estimator $\widehat{\mathcal{E}}_a$:

$$\begin{aligned} T_{abcd} &\equiv \langle \widehat{\mathcal{E}}_a \widehat{\mathcal{E}}_b \widehat{\mathcal{E}}_c \widehat{\mathcal{E}}_d \rangle_{\text{mock}}^{\text{conn}} \\ &= \langle \widehat{\mathcal{E}}_a \widehat{\mathcal{E}}_b \widehat{\mathcal{E}}_c \widehat{\mathcal{E}}_d \rangle_{\text{mock}} - C_{ab}^{\text{mock}} C_{cd}^{\text{mock}} - C_{ac}^{\text{mock}} C_{bd}^{\text{mock}} - C_{ad}^{\text{mock}} C_{bc}^{\text{mock}} \end{aligned} \quad (\text{B.2})$$

Note that $\widehat{\mathcal{E}}_a$ is a four-point function in the underlying galaxy field δ_g , C_{mock} is an eight-point function in δ_g , and T_{abcd} is a 16-point(!) function in δ_g .

A short calculation shows that when we compute $\text{Var}(\chi^2)$, we get two terms:

$$\begin{aligned} \text{Var}(\chi^2) &= \text{Var}[\widehat{\mathcal{E}}_a (C_{\text{ana}}^{-1})^{ab} \widehat{\mathcal{E}}_b] \\ &= \underbrace{2 \text{Tr}[C_{\text{ana}}^{-1} C_{\text{mock}} C_{\text{ana}}^{-1} C_{\text{mock}}]}_{\text{“Gaussian” variance}} + \underbrace{(C_{\text{ana}}^{-1})_{ab} (C_{\text{ana}}^{-1})_{cd} T^{abcd}}_{\text{“non-Gaussian” variance}} \end{aligned} \quad (\text{B.3})$$

We will model these two terms separately. To model the Gaussian variance, we assume that C_{mock} is approximately proportional to C_{ana} , which implies:

$$\text{Tr}[C_{\text{ana}}^{-1} C_{\text{mock}} C_{\text{ana}}^{-1} C_{\text{mock}}] \approx \frac{1}{N_{\text{dof}}} \text{Tr}[C_{\text{ana}}^{-1} C_{\text{mock}}]^2 = N_{\text{dof}} \frac{V_{\text{fid}}^2}{V_{\text{eff}}^2} \quad (\text{B.4})$$

using the definition (B.1) of V_{eff} . We model the non-Gaussian variance by simply assuming that it is approximately proportional to $1/V_{\text{eff}}^3$ (as expected by mode counting). We parameterize the proportionality constant as:

$$(C_{\text{ana}}^{-1})_{ab} (C_{\text{ana}}^{-1})_{cd} T^{abcd} \approx 2N_{\text{dof}} \frac{V_{\text{thresh}} V_{\text{fid}}^2}{V_{\text{eff}}^3} \quad (\text{B.5})$$

where V_{thresh} is a free parameter of our model, with units of volume.

Combining eqs. (B.4) and (B.5), our “bottom-line” one-parameter model for $\text{Var}(\chi^2)$ is:

$$\frac{\text{Var}(\chi^2)}{V_{\text{fid}}^2} \approx \frac{2N_{\text{dof}}}{V_{\text{eff}}^2} \left(1 + \frac{V_{\text{thresh}}}{V_{\text{eff}}} \right) \quad (\text{B.6})$$

We determine the parameter V_{thresh} by fitting to the points in figure 7, obtaining:

$$V_{\text{thresh}} = 6.87 h^{-3} \text{Gpc}^3 \quad (\text{B.7})$$

Note that all regions in figure 7 satisfy $V_{\text{eff}} \lesssim V_{\text{thresh}}$, which implies that $\text{Var}(\chi^2)$ is dominated by the non-Gaussian term in eq. (B.3).

B.2 A zero-parameter model for $\text{Var}(\chi_{\times}^2)$

In this section, we will develop an analytic model for $\text{Var}(\chi_{\times}^2)$, with no free parameters. Consider a survey which is divided into N_p patches. We denote the effective volumes of the survey and the patches by $V_{\text{eff}}^{\text{tot}}, V_{\text{eff}}^{\mu}$. Following section 4.3, we assume that for distinct patches $\mu \neq \nu$, the estimators $\widehat{\mathcal{E}}_a^{\mu}$ and $\widehat{\mathcal{E}}_b^{\nu}$ are uncorrelated. Then, starting from the definition (4.10) of χ_{\times}^2 , a short calculation gives $\text{Var}(\chi_{\times}^2)$:

$$\text{Var}(\chi_{\times}^2) = \frac{2}{N_p^2 (N_p - 1)^2} \sum_{\mu \neq \nu} \text{Tr}[C_{\text{ana}}^{-1} C_{\text{mock}}^{\mu} C_{\text{ana}}^{-1} C_{\text{mock}}^{\nu}] \quad (\text{B.8})$$

To model the trace on the right-hand side, we assume that C_{mock}^μ and C_{mock}^ν are approximately proportional to C_{ana} , which implies:

$$\text{Tr}[C_{\text{ana}}^{-1} C_{\text{mock}}^\mu C_{\text{ana}}^{-1} C_{\text{mock}}^\nu] \approx N_{\text{dof}} \frac{V_{\text{fid}}^2}{V_{\text{eff}}^\mu V_{\text{eff}}^\nu} \quad (\text{B.9})$$

by the same reasoning as in eq. (B.4). It will be convenient to define a ‘‘covering fraction’’ f_{cov} by:

$$f_{\text{cov}} \equiv \left(\frac{1}{N_p^3 (N_p - 1)} \sum_{\mu \neq \nu} \frac{(V_{\text{eff}}^{\text{tot}})^2}{V_{\text{eff}}^\mu V_{\text{eff}}^\nu} \right)^{-1/2} \quad (\text{B.10})$$

To motivate this definition, note that if $V_{\text{eff}}^\mu = f V_{\text{eff}}^{\text{tot}} / N_p$, as intuitively expected for equally sized patches which collectively cover fraction $0 < f \leq 1$ of the survey area, then $f_{\text{cov}} = f$. In practice, the value of f_{cov} will be less than the geometric expectation. We find $f_{\text{cov}} = 0.68$ (0.73) for CMASS-NGC (CMASSLOWZTOT-SGC), whereas the geometric expectation is 0.78 (0.88).

Combining eqs. (B.8) to (B.10), we get our final ‘‘bottom-line’’ prediction for $\text{Var}(\chi_\times^2)$:

$$\frac{\text{Var}(\chi_\times^2)}{V_{\text{fid}}^2} \approx \frac{2N_{\text{dof}}}{V_{\text{eff}}^2} \left(\frac{N_p}{f_{\text{cov}}^2 (N_p - 1)} \right) \quad (\text{B.11})$$

This model for $\text{Var}(\chi_\times^2)$ has no free parameters. This is because $\text{Var}(\chi_\times^2)$ only has a Gaussian term (eq. (B.8)), whereas $\text{Var}(\chi^2)$ has Gaussian and non-Gaussian terms (eq. (B.3)). When we compare the model with measurements of $\text{Var}(\chi_\times^2)$ from mocks, it agrees within $\sim 5\%$ for both surveys (CMASS-NGC, CMASSLOWZTOT-SGC).

B.3 Comparison between $\text{Var}(\chi^2)$ and $\text{Var}(\chi_\times^2)$

Now that we have models for $\text{Var}(\chi^2)$ and $\text{Var}(\chi_\times^2)$, we can compare them. Combining eqs. (B.6) and (B.11) we get:

$$\frac{\text{Var}(\chi^2)}{\text{Var}(\chi_\times^2)} = f_{\text{cov}}^2 \frac{N_p - 1}{N_p} \left(1 + \frac{V_{\text{thresh}}}{V_{\text{eff}}^{\text{tot}}} \right) \quad (\text{B.12})$$

We see that in the large-volume limit $V_{\text{eff}}^{\text{tot}} \gg V_{\text{thresh}}$, we get the inequality $\text{Var}(\chi^2) < \text{Var}(\chi_\times^2)$, as intuitively expected. However, this inequality reverses in the small-volume limit $V_{\text{eff}}^{\text{tot}} \ll V_{\text{thresh}}$, where the non-Gaussian term in $\text{Var}(\chi^2)$ dominates.

The BOSS surveys in this paper are ‘‘small’’ surveys, in the sense that $V_{\text{eff}} \lesssim V_{\text{thresh}}$, so we have found the counterintuitive inequality $\text{Var}(\chi_\times^2) < \text{Var}(\chi^2)$ throughout the paper. The analysis in this appendix has shown that this is a finite-volume effect, i. e. the inequality would be reversed for a larger survey.

C Data and mock investigations

In an early stage of this paper, we looked for systematic inhomogeneities in the BOSS data and mocks which might explain a parity-odd 4PCF. We found a previously unknown systematic effect in the PATCHY mocks (figure 9). We ultimately concluded that the effect was too small to explain the excess χ^2 , but in this appendix we describe the systematic effect that we found.

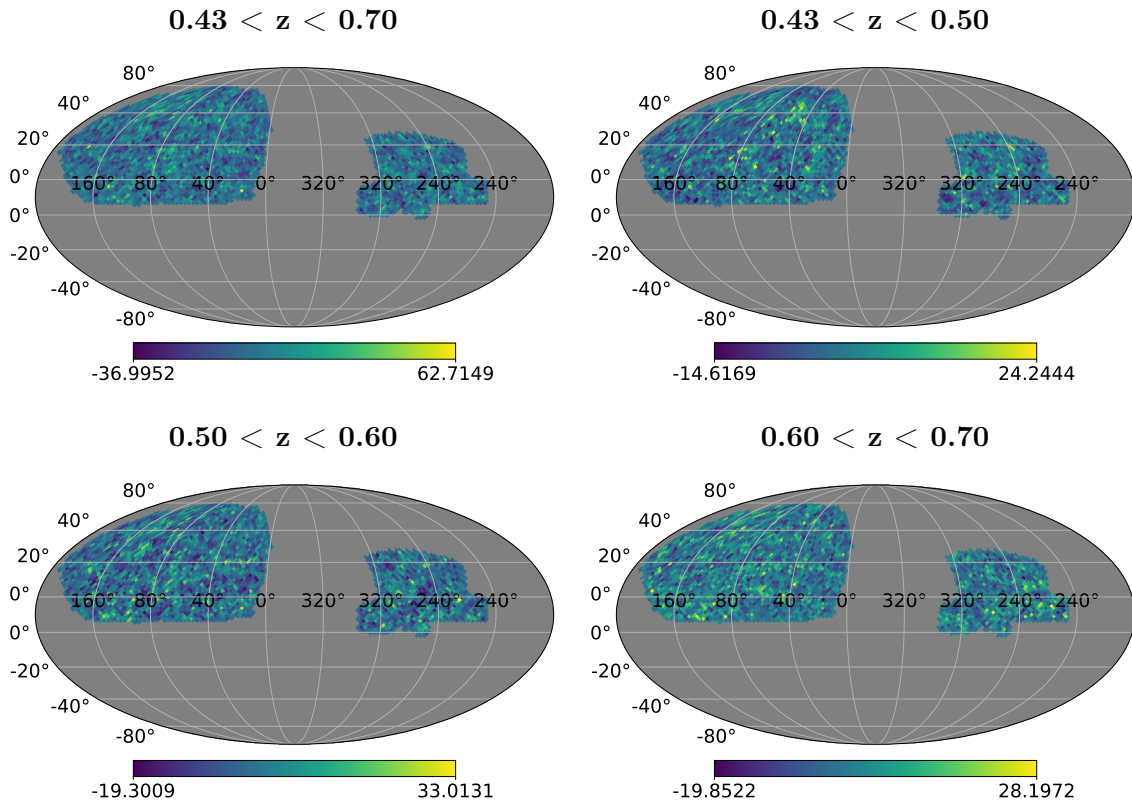


Figure 8. Sky maps of data minus randoms, normalized to sum to zero, for the BOSS data catalog. We show both the entire redshift range as well as three slices in redshift.

We searched for angular inhomogeneities in the BOSS data and mocks by creating sky maps of the data counts minus the random counts, normalized such that the sum of the map is zero. In figure 8, we show these maps for the data, split into three redshift slices. There are no significant artifacts in these plots, i. e. the sky distribution of data and randoms matches.

We show the same plot in figure 9 for the sum of the 2048 Patchy mocks in the NGC. In contrast to the data, there is a striping artifact apparent in the overall redshift range and in each of the redshift slices. The artifact is caused by a 10% reduction in mock data counts within these two stripes on the sky.

We create and apply a mask to remove this stripe from the data and mocks. Testing its impact on the 10-bin results for the first 20 mocks, we find that adding the stripe mask increases χ^2 by 594 for the mocks, on average. It also increases χ^2 by 670 for the data, and hence increases the detection significance from 2.8σ to 3.4σ . We conclude that the striping artifact does not have a significant impact on the parity-odd detection. Moreover, the striping is only present in NGC whereas the parity-odd signal is detected at a similar level in both NGC and SGC, implying that the striping cannot explain the parity-odd detection.

D Condition number and eigenvalues of the analytic covariance

In an early stage of this paper, we noticed that the analytic covariance matrix $(C_{\text{ana}})_{ab}$ is poorly conditioned. We wondered whether this could make the statistic $\chi^2 \equiv \hat{\mathcal{E}}_a (C_{\text{ana}})^{ab} \hat{\mathcal{E}}_b$

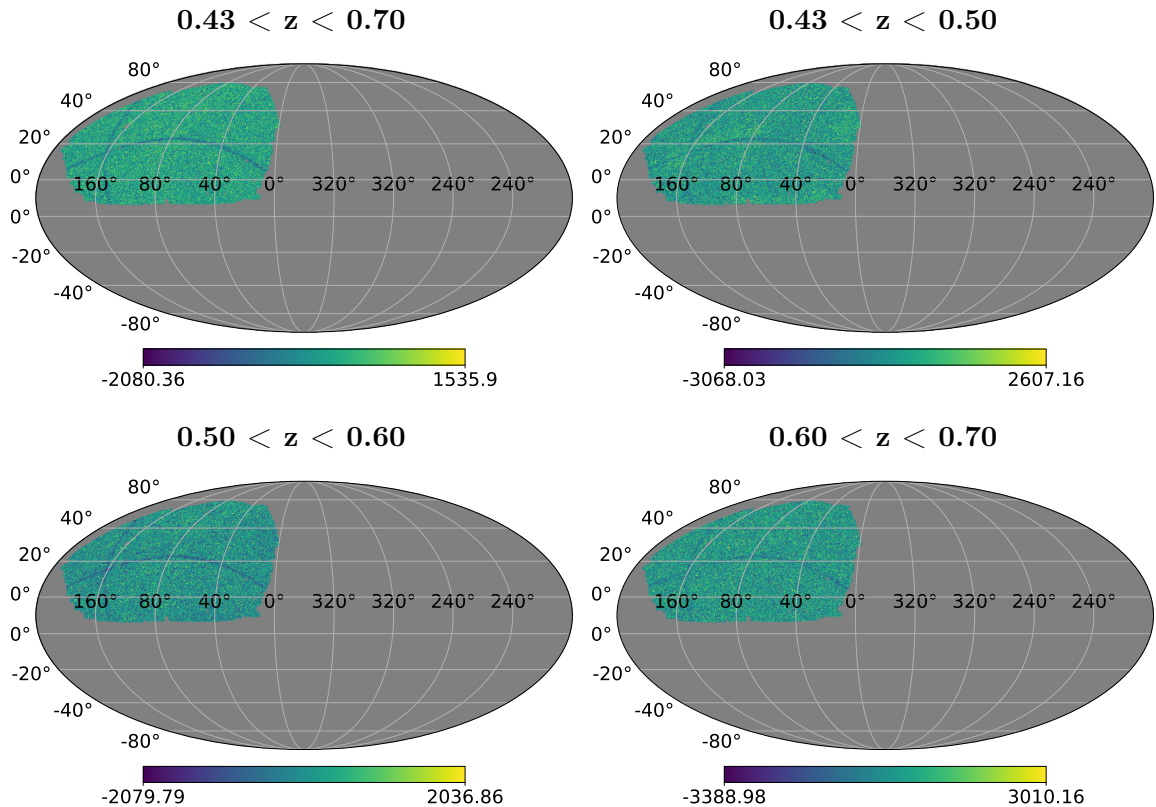


Figure 9. Sky maps of data minus randoms, normalized to sum to zero, summed over the 2048 Patchy mocks in the NGC. Visible striping artifacts are present. We show both the entire redshift range as well as three slices in redshift.

susceptible to small effects such as imperfect edge correction, explaining the χ^2 excess. In this appendix, we show that for the 10-bin and 18-bin cases considered in this paper (see section 3.1) the poor conditioning is unlikely to be an issue.

In figures 10 and 11, we plot the eigenvalues of the correlation matrix for the 10-bin and 18-bin analytic covariance matrices. We also show the contributions to χ^2 from each eigenmode of the correlation matrix $R_{ab} \equiv (C_{\text{ana}})_{ab} / \sqrt{(C_{\text{ana}})_{aa}(C_{\text{ana}})_{bb}}$. More precisely, we write $C_{\text{ana}} = DRD$ where D is diagonal, and diagonalize $R = U\Delta U^T$ where Δ is diagonal and U is unitary. Then $\chi^2 = \tilde{d}\Delta^{-1}\tilde{d}$ where $\tilde{d} = U^T D^{-1}d$. Since Δ is diagonal, we can therefore write χ^2 as a sum and decompose its mode-by-mode contributions. The mode-by-mode contributions to χ^2 are extremely noisy, so we average them in relatively large blocks for convenience when plotting. In figures 10 and 11, we show the mode-by-mode contributions for both data and mocks, for the 10-bin and 18-bin cases. While the range in the eigenvalues is quite large (particularly in the 18-bin case), the χ^2 contribution is similar from all eigenmodes, suggesting that the high condition number is not leading to numerical instability in the χ^2 statistic.

E Comments on related null tests from [1, 2]

Our new statistic χ_{null}^2 is a null test, in the sense that statistical deviation from zero is evidence for systematics or data-mock mismatch (not parity violation). In section 4.4, we

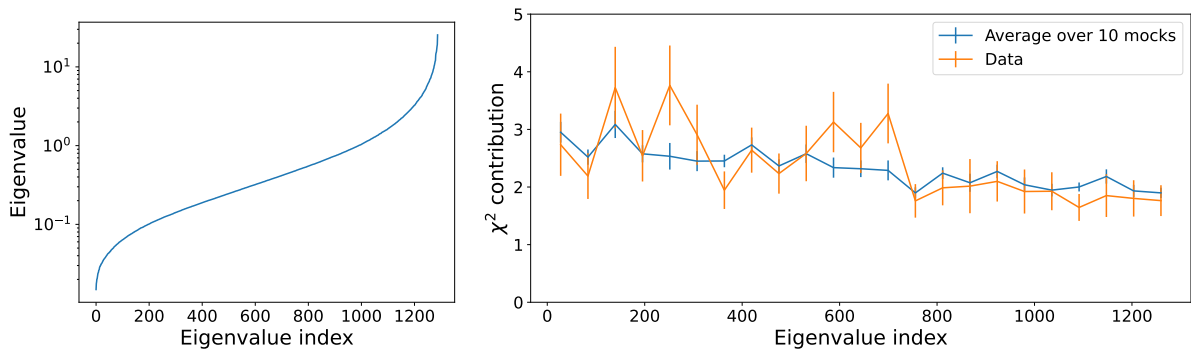


Figure 10. *Left:* Distribution of eigenvalues of the correlation matrix for the 10-bin analytic covariance in the BOSS CMASS-NGC region. *Right:* Mode-by-mode contribution to the χ^2 for both data (orange) and average over 10 mocks (blue), averaged over blocks of 56 eigenvalues to reduce noise.

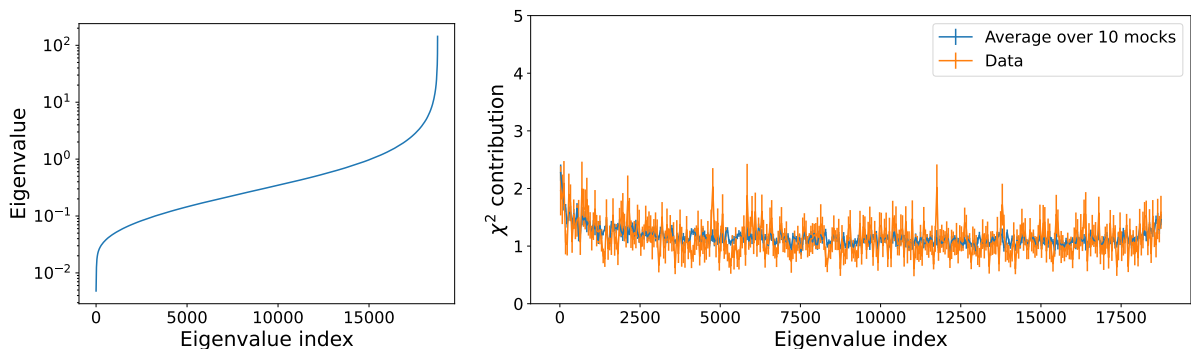


Figure 11. Same as figure 10, but for the 18-bin case. The averaging is done in blocks of 51 eigenvalues.

found that this null test failed at 5.6σ or 6.8σ , for CMASS-NGC or CMASSLOWZTOT-SGC respectively. The reader may wonder how this high-significance null test failure relates to the null test suites from [1, 2], where no clear null test failure was found. In this section, we will comment on three null tests from [1, 2] that resemble our new statistics ($\chi^2_x, \chi^2_{\text{null}}$), and explain why these null tests did not detect data–mock mismatch.

E.1 Matching the 4PCF between data and mocks

First, we consider the “realization-dependent amplitude” from section VI.C of [2]. In this test, the parity-odd 4PCF $\hat{\mathcal{E}}_a$ is rescaled by an overall constant factor A , which is based on the amplitude of the parity-even 4PCF. We expect that this procedure may ameliorate data–mock mismatch to some extent, since it can compensate for systematic differences in the 4PCF between data and mocks. However, the χ^2 -statistic is biased by the difference in 8PCFs between data and mocks eq. (1.7). Even if the 4PCFs of the data and mocks agree perfectly, there is no guarantee that the 8PCFs are equal. Therefore, the realization-dependent amplitude test does not conclusively address the issue of data–mock mismatch.

There is a similar test in section 4.2.3 of [1], where the covariance is rescaled instead of the 4PCF. This reduces the detection significance to 2σ (4.6σ) when rescaling the covariance

so that the parity-even 4PCF agrees at 1σ (3σ) between mocks and data. However, this still does not exclude the possibility of an 8PCF bias driving the residual χ^2 detection.

E.2 Comparing χ^2 in different patches of sky

In section 6.1.6 of [4] and in section VI.A of [2], there is a null test based on comparing values of χ^2 in different patches of sky. These patch-based null tests resemble the analysis in our paper, but there is one key difference. Our null test χ_{null}^2 is based on comparing the parity-odd four-point function $\widehat{\mathcal{E}}_a$ in different sky patches, *before* $\widehat{\mathcal{E}}_a$ is squared to obtain χ^2 (eq. (4.15)). On the other hand, the patch-based null tests from [1, 2] are based on comparing values of χ^2 (after squaring) in different sky patches. These are different null tests, and may succeed or fail independently of each other. We expect that χ_{null}^2 is more sensitive to covariance mismatch ($C_{\text{data}} \neq C_{\text{mock}}$), whereas the patch-based tests from [1, 2] is more sensitive to systematics which break statistical isotropy.

E.3 The r_p -statistic (correlating NGC and SGC)

In section 5.2 of [1], there is a statistic r_p which is very closely related to our statistic χ_{\times}^2 . The r_p -statistic is defined for a survey with $N_p = 2$ patches. In [1], the patches are chosen to be the NGC and SGC. To define r_p , it will be convenient to diagonalize $C_{\text{ana}} = R^T \Lambda R$, and change variables from $\widehat{\mathcal{E}}_a^\mu$ to the length- N_{dof} “data vector” d_a^μ defined by:

$$d_a^\mu = (\Lambda^{-1/2} R)_{ab} \widehat{\mathcal{E}}_b^\mu \quad (\text{E.1})$$

Then r_p is defined to be the correlation coefficient between the data vectors $d_a^{(1)}$, $d_a^{(2)}$:

$$r_p \equiv \frac{\sum_a (d_a^{(1)} - \bar{d}^{(1)})(d_a^{(2)} - \bar{d}^{(2)})}{\sqrt{(\sum_a (d_a^{(1)} - \bar{d}^{(1)})^2)(\sum_b (d_b^{(2)} - \bar{d}^{(2)})^2)}} \quad \text{where } \bar{d}^{(i)} \equiv \frac{1}{N_{\text{dof}}} \sum_{i=1}^{N_{\text{dof}}} d_a^{(i)} \quad (\text{E.2})$$

In [1], the statistic r_p is found to be statistically consistent with zero, but section 5.2 of [1] argues that this *does not* rule out parity violation. On the other hand, in this paper, we find that χ_{\times}^2 is statistically consistent with zero, but we show that this *does* rule out parity violation. One may wonder how these statements can be consistent, since the statistics χ_{\times}^2 and r_p are so conceptually similar.

To answer this question, we first note that our χ_{\times}^2 statistic can be written in “data vector” notation as follows:

$$\chi_{\times}^2 = \sum_a d_a^{(1)} d_a^{(2)} \quad (\text{E.3})$$

Comparing eqs. (E.2) and (E.3), we see that the r_p -statistic differs from χ_{\times}^2 in two ways: r_p is defined with \bar{d} -subtraction, and r_p is defined with a denominator which ensures $r_p \in [-1, 1]$.

The denominator of eq. (E.2) is not important (as far as we can tell), but the \bar{d} -subtraction in the numerator has an important consequence. Consider the following toy model of parity violation:

$$\langle d_a^\mu \rangle = C \quad (\text{where } C \text{ is a constant independent of } a, \mu) \quad (\text{E.4})$$

In this toy model, the statistic χ_{\times}^2 is sensitive to the value of C , but the statistic r_p is not sensitive to C because of the \bar{d} -subtraction in the definition (E.2).

This toy model shows that it is possible for parity violation to make a large contribution to χ^2 , but a small (or even zero) contribution to r_p . For this reason, [1] concluded that a small value of r_p is inconclusive, and does not rule out parity violation. (The argument in section 5.2 of [1] is based on a different toy model than (E.4), but the principle is the same.)

This issue does not arise for the χ^2_{\times} statistic, which is defined without \bar{d} -subtraction (eq. (E.3)). If parity violation makes a statistically significant contribution to χ^2 , then it must also make a statistically significant contribution to χ^2_{\times} . This follows formally from eqs. (4.9) and (4.13), which show that the statistics χ^2 and χ^2_{\times} have the same expectation value $\bar{\mathcal{E}}_a (C_{\text{ana}}^{-1})^{ab} \bar{\mathcal{E}}_b$ due to parity violation, plus the statement that $\text{Var}(\chi^2_{\times}) \lesssim \text{Var}(\chi^2)$. (See appendix B for more discussion of this latter statement.)